Available online at www.sciencedirect.com
ScienceDirect
Thermochimica Acta 461 (2007) 14–43
thermochimica acta
www.elsevier.com/locate/tca

Review

Vibrational and relaxational properties of crystalline and amorphous ices

G.P. Johari [a,*], Ove Andersson [b]

[a] *Department of Materials Science and Engineering, McMaster University, Hamilton, Ontario L8S 4L7, Canada*
[b] *Department of Physics, Umeå University, 901 87 Umeå, Sweden*

Available online 24 March 2007

Abstract

Pure water forms 15 crystalline ices at different temperatures and pressures, and its solutions containing small molecules form three crystallographically distinct clathrates. Its vapours deposited on a substrate at $T < 100$ K produce a porous amorphous solid and pure water vitrifies ($T_g = 136$ K) when hyperquenched in micron-size droplets. At a temperature below 140 K, hexagonal and cubic ice collapse when pressure exceeds ∼1 GPa to a ∼30% denser amorphous solid, which on heating at ambient pressure transforms to an amorphous solid with density similar to that of hexagonal ice. In this essay, we describe (i) the thermal conductivity of the ices and clathrates and the thermal conductivity and heat capacity of water's amorphous solids, their thermodynamic paths and their transformations, and (ii) the dielectric relaxation time of ultraviscous water formed on heating the amorphous solids. We also describe the characteristics of pressure collapse and subsequent amorphization of hexagonal and cubic ices that occurs over a period of several days according to a stretched exponential kinetics and a pressure-, and temperature-dependent rate constant. This process is attributed to the production of lattice faults during deformation of the ice and the consequent distribution of the Born instability pressures. This ultimately produces a kinetically unstable high-energy amorphs in the same manner as random deformation of crystals produces kinetically unstable high-energy amorphs, with density and properties depending upon their temperature–pressure–time history. On heating at 1 GPa pressure, the pressure-amorphized solid relaxes to a lower energy state, becoming ultraviscous water at 140 K. But on heating at ambient pressure, it irreversibly transforms slowly to a low-density amorph that differs from glassy water and vapour-deposited amorphous solid.

Keywords: Ices; Amorphous solid and glassy water; Thermal conductivity; Heat capacity; Dielectric relaxation; Amorphization mechanism

Contents

* Corresponding author.
E-mail address: joharig@mcmaster.ca (G.P. Johari).

0040-6031/$ – see front matter © 2007 Elsevier B.V. All rights reserved.
doi:10.1016/j.tca.2007.03.011

1. Introduction

Pure water is known to form 15 crystalline phases. It is believed that it forms also at least three amorphous solids, although like any amorphous solid state of a material, the number of its amorphous solids may be virtually infinite. The crystalline phases have been named hexagonal ice (ice Ih) and cubic ice (ice Ic), both of which are bulkier than water, and ices II–XII, as reviewed in Ref. [1], and two recently found phases ices XIII [2] and XIV [3] all of which are denser than water. Regions of their thermodynamic stability and the metastable conditions in which ices Ic, IV and XII have been formed are shown in the temperature–pressure phase diagram in Fig. 1. Ice X, which is not shown, has a centrosymmetric structure of hydrogen bonds. It forms at pressures higher than ∼44 GPa [4]. At ambient pressure, bulk water freezes to ice Ih, but sub-micron size droplets of pure water freeze to ice Ic, as described in Ref. [5]. Only ices III–VII and XII have been made by compressing bulk water and therefore these are shown to have a phase boundary with liquid water, except ice XII. Ice IV is formed by nucleation with organic molecules [6] and it is a metastable phase in the temperature and pressure range of ice V. Ice XII is also a metastable phase formed directly from water in the presence of silica fibres which presumably act as a nucleating surface [7]. Many of the high-pressure ices have recently been produced by crystallization of a high-density apparently amorphous solid water or by heating the metastable ice XII [8].

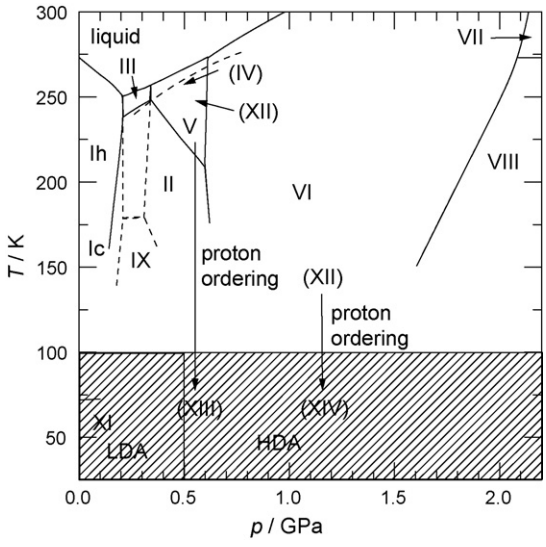

Fig. 1. Phase diagram of water and ice showing the regions of stability of 15 crystalline phases and three amorphous phases. The amorphous phases have been made by hyperquenching of water, pressure-amorphization of ices Ic and Ih and heating of the pressure-amorphized solids. H_2O molecules are orientationally disordered in the structure of metastable ice Ic, and also in the structure of all those stable or metastable ices that have an equilibrium phase boundary with liquid water, even when they form in the domain of another ice by freezing water containing nucleating agents. All of these hydrogen-atoms or protons disordered phases have a finite configurational entropy. All these ices are expected to become orientationally ordered on cooling with a change in the crystal symmetry. The shaded region of the diagram is for the temperature–pressure range in which high-density and low-density amorphs and hyperquenched glassy water are stable for a long enough period to be studied.

In the crystal structures of the ices, each H_2O molecule forms four hydrogen bonds with its four neighbours. Two hydrogen bonds are formed by a molecule donating protons, one each to two neighbouring H_2O molecules, and two by accepting protons, one each from the other two neighbouring H_2O molecule [9]. Thus, an H_2O molecule is hydrogen-bonded in a tetrahedral arrangement in the ice structures, resembling the structure of covalent bonds in silica. The angle between the oxygen atoms of the H_2O molecules in ices Ih, Ic and VIII is nearly tetrahedral and the hydrogen bonds between two H_2O molecules are linear. This angle varies greatly in other ices and the hydrogen bonds between two H_2O molecules are non-linear. This variation allows for the increase in the density of their structures. In the crystal structure of all the ices that form directly by cooling water, H_2O molecules at the lattice sites are randomly oriented. Therefore, these ices are said to be orientationally disordered, or proton-disordered. There is no long-range order for the hydrogen atom positions in their structures. It is probably correct to say that ice Ih is the most abundant orientationally disordered crystal phase on the Earth and in its atmosphere, and clouds occasionally contain crystals of ices Ih and Ic along with water droplets and water vapour.

Because of the orientational or proton-disorder of H_2O molecules, ices Ih, Ic, III–VII and possibly XII have a finite value of the configurational entropy. The maximum value of this entropy is equal to $R\ln(3/2)$ (=3.27 J (mol K)$^{-1}$), where R is the gas constant [1]. Except for ice II that forms by varying the temperature and/or pressure of ices Ih, Ic, III and V, the remaining crystalline phases, ices VIII, IX, XI, XIII and XIV are made by orientationally ordering, or proton-ordering, of respectively, ices VII, III, Ih, V and XII. Ice VIII forms gradually on cooling of ices VII and IX on cooling of ice III, whereas orientational ordering of ice Ih is achieved by isothermal, long time annealing of the pure or doped ice Ih to produce, somewhat slowly, significant amounts of ice XI. Ice X is produced by pressurizing ice VII at 100 K to above 62 GPa. In its structure, protons are symmetrically placed between two oxygen atoms [1]. Finally, ice XIII [2] and ice XIV [3] have been produced by cooling of HCl-doped ices V and XII, respectively, and the transformation has been found to be thermally reversible in a short duration.

Water containing certain small molecules freezes to produce crystals of ice clathrates. In their structure, H_2O molecules form hydrogen bonds to produce cage-like structures which confine the small molecules. Three such crystalline forms of clathrates are known, two have cubic structures in different space groups [10,11] and one hexagonal [12]. Some of the clathrates contain methane and other hydrocarbons, and are found to occur in vast quantities in the cold regions of the Earth and in submarine sediments [13–15]. Recently, it has been found that clustered hydrogen molecules can be stored in the cages of the clathrate structures [16–18]. These clathrates are of practical importance [19,20].

Water also forms at least three amorphous solids. The oldest known amongst these was made by depositing water vapours on a substrate held at a temperature below 100 K [21]. As formed,

this solid is relatively porous and it exothermally anneals on heating [22]. Water droplets of less than 3 μm diameter dispersed as an aerosol in N_2 gas have been rapidly quenched to 77 K to produce 2–3 mm-thick opaque layer of hyperquenched glassy water [23–25]. In their annealed states both the vapour-deposited amorphous solid and hyperquenched glassy water show identical thermodynamic behaviours, the same T_g of 136 K for the heating rate of 30 K min^{-1} [26] and become ultraviscous water at 140 K. The other two forms of amorphous solid water have been produced by pressurizing ices Ih and Ic at a temperature below 140 K to ∼1 GPa [27–33]. The density of the pressure-amorphized state thus obtained by the collapse of the (bulkier) ices Ih and Ic structures is 1.17 g ml^{-1} at ambient pressure and 77 K [27]. This solid has therefore become known as the high-density amorph or HDA. Studies in recent years have shown, and it is now agreed, that the term HDA is generic. It refers to all amorphous solids of unknown density produced by pressure collapse of ices Ih and Ic at different temperature, pressure, and time conditions [34–36]. When this solid HDA is recovered at ambient pressure and is then heated at ambient pressure, it transforms irreversibly (and exothermally) to another amorphous solid whose density is 0.93 g ml^{-1} at 77 K [28], which is similar to the density of ices Ih and Ic. Because of its low-density, this third form has been called the low-density amorph (LDA). When LDA at a low temperature is pressurized to ∼0.4 GPa, it converts to HDA. A thermodynamic state analysis has shown that this HDA differs from the HDA formed by pressurizing ice Ih to 1 GPa [37]. When LDA is heated at ambient pressure, it transforms exothermally to ice Ic with negligible change in the density. Amorphous solid water has been found occasionally in the atmosphere, and it is estimated that large quantities of both crystalline and amorphous solid forms of water are present in the nuclei of comets and interstellar dust, and in satellites and giant planets [38–43].

Crystalline and amorphous solid states of water are remarkable examples of hydrogen bonding and are therefore of general interest. They are also of practical importance in the discipline of cryobiology, food sciences, astrophysics and geophysics of planets and satellites. In this essay we describe some of the vibrational properties of the ices, as well as of water's amorphous solids, particularly their thermal conductivity and heat capacity. We also describe how calorimetry and dielectric spectroscopy have been used for characterizing crystalline and amorphous solids and discovering new forms. Finally, we describe the mechanism of pressure-amorphization of ices Ih and Ic, and the thermodynamics and relaxation of the amorphous forms. As the emphasis here is on thermal properties, most of the information on water's amorphous solids obtained by X-ray and neutron scattering studies is excluded. For the sake of completeness, we include a brief description of the rather unusual experimental methods used for measuring the thermal conductivity, heat capacity and dielectric relaxation time of these solids at high pressures and low temperatures. Studies of the water's amorphous solids by diffraction methods and by computer simulation have been reviewed recently [44], and therefore are mentioned only briefly here.

2. Experimental methods for measurements at high pressures

In our studies of water and other materials, a hot-wire method has been used to measure both the thermal conductivity, κ, and the product of the density and heat capacity [34,45–50]. The method is based on a mathematical solution of the time-dependent equation for heat conduction and has been described in detail earlier [51]. In this solution, the temperature rise ΔT of an infinitely long, infinitely conducting wire immersed in an infinitely large specimen is given by [52]

$$\Delta T = \frac{2q\alpha^2}{\pi^3\kappa} \times \int_0^\infty \frac{1-\exp(-\beta u^2)}{u^3\{(uJ_0(u)-\alpha J_1(u))^2+(uY_0(u)-\alpha Y_1(u))^2\}}\,du, \quad (1)$$

where q is the constant heating power input per unit length, $\alpha = 2\rho C_p/(\rho_w C_w)$, $\beta = \kappa t/(\rho C_p r^2)$, t the time, r the radius of the hot-wire, ρ and C_p the density and heat capacity of the specimen, ρ_w and C_w the density and heat capacity of the hot-wire, J_0 and J_1 Bessel functions of the first kind of zero and first order, and Y_0 and Y_1 are Bessel functions of the second kind of zero and first order.

The hot-wire sample cell, illustrated in Fig. 2(A), is made of Teflon. The hot-wire itself is a 0.1 mm diameter 40 mm long Ni-wire. The Teflon container is ∼30 mm deep and 37 mm internal

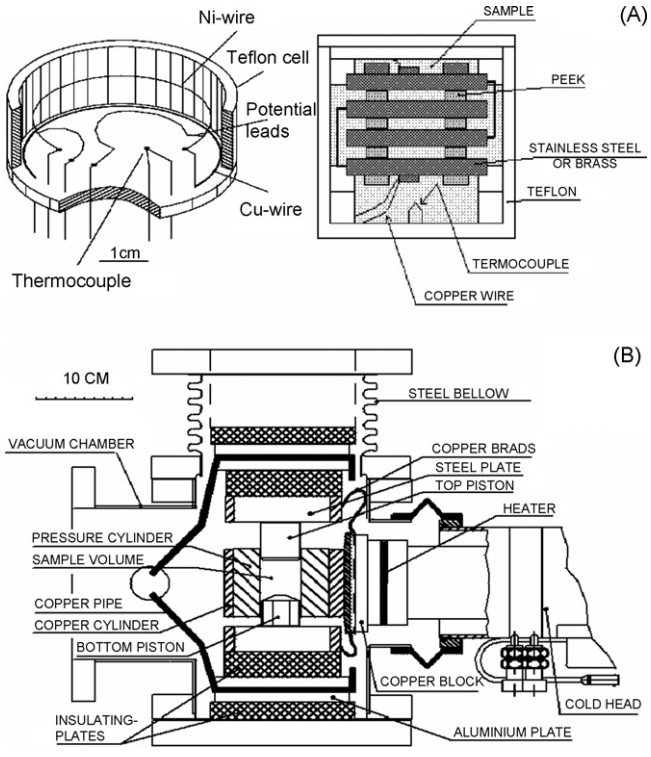

Fig. 2. (A) The high-pressure cell assembly for measuring the thermal conductivity and heat capacity (left) and the dielectric relaxation time (right). (B) The arrangement of the high-pressure vessel showing the application of the uniaxial stress and arrangement that allows the use of helium cryostat in a massive assembly.

diameter with a tightly sealing Teflon cover. It closely fits inside the piston-cylinder assembly of internal diameter 45 mm of a high-pressure assembly illustrated in Fig. 2(B). In order to best use the limited space available in high-pressure equipment, the wire is placed horizontally in a ring of constant radius within the Teflon cell. At each heating event, the hot-wire probe, which is surrounded by the material under investigation, is heated by a 1.4 s long pulse of nominally constant power during which the wire resistance is measured as a function of time. The temperature rise of the wire is then calculated by using the relation between its resistance and temperature, i.e. the wire acts as both the heater and the sensor for the temperature rise. Eq. (1) for the temperature rise with time is fitted to the data points for the hot-wire temperature rise, thereby yielding κ and ρC_p. The inaccuracy in κ and ρC_p thus measured are $\pm$2% and $\pm$5%, respectively, at 298 K. It should be stressed that for measuring κ and ρC_p by this method the wire and the sample must remain in good thermal contact. In the studies of the ices and amorphous solid water, good thermal contact with the hot wire is ensured only at pressures higher than $\sim$0.05 GPa, and therefore the low-pressure limit of the study is 0.05 GPa. Also, as the temperature coefficient of electrical resistance of the nickel hot-wire decreases with decrease in the temperature, the inaccuracy of κ measurements increases to about $\pm$4% at 40 K. The standard deviations of the data obtained in these measurements are an order of magnitude smaller than the inaccuracy.

Dielectric measurements at high pressures are performed by using two types of dielectric cells, one is a parallel plate capacitor of nominally 125–150 pF air capacitance, and the second a concentric electrode capacitor of nominally 19 pF air capacitance [53,54]. The parallel plate capacitor consists of six plates constructed from either stainless steel or brass, each separated from the other by poly(ether-etherketone) spacers. A similar capacitor but only with four plates is illustrated in Fig. 2(A). The concentric electrode cell is constructed from a Cu alloy. The capacitor used in the study is placed inside the Teflon container described above, filled with water, sealed with the Teflon cover and inserted into the high-pressure piston-cylinder apparatus in which it fitted closely. The capacitance and conductance of the dielectric capacitor immersed in the ice sample are measured by means of a Solartron 1260 impedance analyser in the frequency range of 100 Hz to 1 MHz. For measurements at frequencies in the range 10 mHz to 100 Hz, a Hewlett-Packard model 33120A function generator is used to provide a sinusoidally varying signal to both the capacitor containing the sample and a reference capacitor placed in series. The voltages over the capacitors are measured simultaneously by two Hewlett-Packard 3457A voltmeters during at least one period by collecting 100 data points, and the capacitance and conductance of the sample are determined for each frequency. The measurement assembly is based on the one used by Forsman [55], but with a new function generator and electronics.

The limiting high-frequency dielectric permittivity ε_∞ and dielectric loss during the pressure collapse of ice Ih and the effect of similar pressure increase on an ice clathrate were measured by Johari and Jones [56] who used a concentric electrode capacitor with the cell constructed from a 2% Be–Cu alloy with the outer electrode acting also as a pressure vessel. In their study the inter-electrode distance increased with increase in pressure, which changed the cell geometry by an amount that had been estimated earlier in the study of dielectric properties of ice VI and later of ice V, where details may be found [57,58]. A similar change in the geometry of the concentric electrode cell had occurred also on raising the pressure from ambient to 1 GPa in our studies. For reasons given earlier [56–58], this change is regarded as insignificant. After including the measurement errors, the dielectric permittivity and loss measured at high pressures are accurate to better than 3%.

In the general experimental procedures for measuring κ, ρC_p and dielectric properties, the Teflon cell is filled with $\sim$20 ml of pure water (tissue-culture grade water purchased from Sigma–Aldrich, or the water purified by using Milli-Q® Ultrapure WaterSystems) and then sealed with a tightly fitting, 5 mm thick, Teflon cover. This hermetically sealed assembly is mounted inside a piston-cylinder type pressure vessel of 45 mm internal diameter, as illustrated in Fig. 2(B) and the load is applied using a hydraulic press. The whole pressure vessel is kept under vacuum and cooled by the refrigerator using a closed helium gas cycle, as illustrated in Fig. 2(B) and described earlier [59]. Pressure is determined from the load/area with a correction for friction which is established using the pressure dependence of the resistance of a manganin wire. The inaccuracy in pressure is estimated as $\pm$40 MPa at 1 GPa and 298 K and, due to increased friction, $\pm$60 MPa at 40 K and 1 GPa. The temperature is measured inside the Teflon cell by using an internal chromel–alumel thermocouple. The inaccuracy in temperature is estimated as $\pm$0.5 K.

This high-pressure assembly and equipment for measuring the dielectric properties, κ and ρC_p, also allows one to measure continuously the temperature difference between the sample and the Teflon cell wall. This is equivalent to differential thermal analysis performed at a very slow heating rate. Thus very slow crystal–crystal transformation and crystal amorphization can also be studied with ease simultaneously with the κ, ρC_p and dielectric measurements. For caution, it should be noted that experiments on pressure-amorphization of ice in this assembly are particularly prone to failure because the slow rate of pressure and temperature change causes the amorphous solid to frequently crystallize, particularly in the broad pressure-amorphization range of 0.8–1.1 GPa. In our experience an average of only one in five experiments is successful in providing the required data. This has not been the case in the studies by other groups who have used $\sim$10 times higher pressurization and cooling rates, and in which the pressure in most studies was raised from 0.1 MPa to 1.5 GPa in 5 min.

3. Vibrational properties of the crystalline and amorphous ice

3.1. The thermal conductivity of crystalline and amorphous solid water

Like a normal crystal, an amorphous solid at low temperatures has no configurations available to its structure. Therefore,

its properties are seen to be entirely vibrational in origin. These are determined mainly by the intermolecular distances, which usually decrease with increase in density as the pressure is increased or the temperature is decreased. In this respect, the phonon heat capacity, C_p, of an amorph changes in a manner similar to that of a crystal, i.e. decreases with decrease in temperature T and increase in pressure p. But as structural disorder changes the mean free path for propagation of phonon with temperature differently from that in a crystal and other phonon scattering modes become prominent, thermal conductivity, κ, of amorphous solids changes quite differently from those of the crystalline state. It seems that of all the non-configurational thermodynamic properties of solid states of water, only κ of its crystalline and amorphous solids has been studied in detail at high pressures. It was done by the Umea University group as part of their comprehensive study of the solid forms of water, of the equilibrium crystal–crystal, irreversible crystal–noncrystal, and noncrystal–crystal transitions, as well as crystal melting. They have also studied the effect of temperature on κ of water's crystalline and amorphous solid phases. Since the magnitude of κ depends upon both the frequency of phonons and the distance of their propagation through the structure of a material, first we describe its characteristic features.

For convenience of discussion, the measured κ data for the solid forms of water and liquid water are plotted against the temperature in Fig. 3, together with the results previously reported by Ross et al. [45–47]. The various solids and liquid water are indicated next to the plots. Of the total of 15 crystalline phases of water, κ of all except ices IV, X, XIII and XIV has been studied. It now seems that κ of ice XII had probably been studied recently [49], but as it still needs a confirmation of the ice structure by determining the diffraction studies of the sample, we have referred to it as metastable ice/ice XII in Fig. 3.

A cursory examination of Fig. 3 shows that κ of the ices is determined not only entirely by their density and structure,

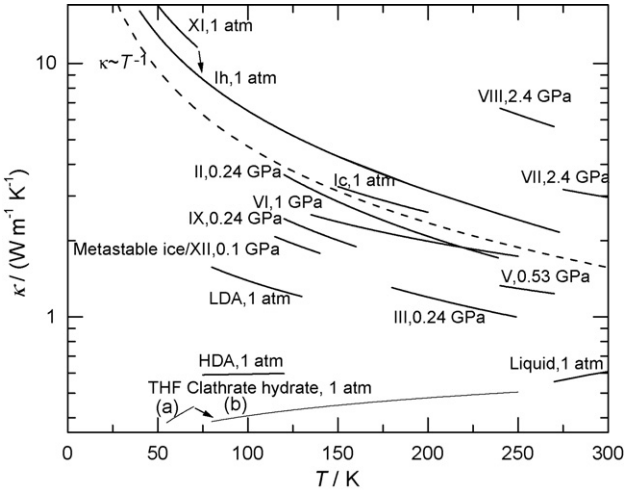

Fig. 3. Thermal conductivity of most of the crystalline ices, the ice clathrate containing tetrahydrofuran as guest molecules in the (a) ordered and (b) disordered states, and two amorphous solid phases of water is plotted against the temperature. The crystalline and amorphous ices and the pressure at which measurements were made are as indicated. Data are taken from Refs. [46–50,67].

which in turn determine the phonon frequencies, but also by the Umklapp scattering and other anharmonic effects that decrease κ. For example, the higher density ice V (1.23 g cm^{-3} [60]) has a lower κ than the lower density ice I (0.93 g cm^{-3}), as seen in Fig. 3, and ice VIII with a higher density (1.46 g cm^{-3} [60]) has a higher κ value than ice V. More clearly, ice Ih and ice Ic have the same density, phonon frequency and heat capacity, and yet κ of ice Ic is remarkably less than that of ice Ih. Thermal conductivity of an ice clathrate containing tetrahydrofuran as guest molecules in the proton-ordered state is plotted as curve (a) in Fig. 3, and in the proton-disordered state in curve (b). The plots show that κ of the ice clathrate is the lowest amongst all the solid forms of water and appears to be somewhat continuous with κ of liquid water at higher temperatures. Since κ has been found to depend only weakly on the crystal structure of a clathrate and also weakly on the type of guest molecules in its symmetrical cages [61,62], it seems that κ of the ice clathrates would be generally lowest among these solids.

As is seen in Fig. 3, κ and its temperature dependence is characteristic of the ice crystalline phases and that different crystalline phases can be distinguished by both the magnitude of κ and its temperature dependence. The thermal conductivity values are well described by an empirical relation, $\kappa \sim T^{-x}$, where x is a constant specific to the ice and its value for different ices is in the range 0.6–1.4 [33]. Such temperature dependence is typical for crystalline phases [62]. Moreover, theoretical discussions have concluded that κ of mono-atomic crystals at temperatures near and above their Debye temperature would vary linearly with the reciprocal temperature. In terms of the Debye theory, this temperature dependence is written as [63]

$$\kappa = \frac{1}{3}\rho C v^2 \tau_s \tag{2}$$

where C is the specific heat capacity contribution from phonons, v the phonon velocity and τ_s is the time between scattering events. At high temperatures, above the Debye temperature, the main source for phonon scattering is known to be three-phonon Umklapp scattering [64]. In such a process, two phonons combine into a third, which has a wave vector that is outside the first Brillouin zone. Consequently, this phonon is physically equivalent to a phonon inside the Brillouin zone, which moves in a significantly different direction than that indicated by the vector sum of the original two phonons. The number of phonons with energies near the Brillouin zone boundaries, which can participate in such an event, increases proportionally to temperature. It follows that the probability for Umklapp scattering events increases proportionally with T and the time between scattering, or the Umklapp scattering time, which is now equal to τ_s varies as T^{-1}. As the quantities ρ, C and v in Eq. (2) vary with the temperature much less than τ_s, this leads to the relation, $\kappa \sim T^{-1}$.

However, deviations from the $\kappa \sim T^{-1}$ relation have been commonly observed in crystalline solids [62,63], and in some cases the deviations are relatively strong. This is the case also for the crystalline ices, as is evident in Fig. 3, which seem to follow the variation, $\kappa \sim T^{-x}$, with x in the range 0.6–1.4. The deviations of course are related to the structure of the ices and the

hydrogen bonding in them, and it is not expected that they would follow the Debye theory for thermal conductivity. Nevertheless, for ices Ih, II and XI, the value of x is close to 1, and therefore they seem to follow the Debye equation. Thermal conductivity of ice VIII has an unusually strong temperature dependence as indicated by the high value of 1.4 for its x. For ices Ic, III, VII, and IX, x is in the range 0.8–0.9, which is a weaker temperature dependence than that expected from the Debye equation, $\kappa \sim T^{-1}$. For the metastable phase ice XII, and high temperature stable phases of ices V and VI, x is in the range 0.6–0.8 which indicates the weakest temperature dependence. Despite the anticipated less validity of the Debye equation for most of the ices, the stronger temperature dependence of κ on T, i.e., when $x > 1$, may be attributed to the higher-order phonon processes and/or to a finite thermal expansion which is determined by the anharmonic forces, whereas a weaker temperature dependence is attributed commonly to scattering arising from structural disorder. The reason for these differences is not well established but one source for a low value of x can also be a somewhat poor crystallinity and/or the orientational-disorder in the structure of some of the ices. However, the latter possibility seems to be excluded by the finding that the large x for the orientationally disordered ice Ih is almost the same as for the orientationally ordered ice XI [48].

Thermal conductivity of a liquid and solid is known to almost invariably increase with its density, and a high-density crystalline phase has often been found to have a higher κ than a low-density crystalline phase [65]. But κ of ices Ih and Ic has been found to decrease with increase in pressure at a fixed temperature, making these two as exceptions to this general pattern of behaviour. In relation to the crystalline ices, with increasing density, κ of ices VII and VIII, the highest density phases, is higher than of all other phases, and despite the same density of the two, κ of the orientationally ordered ice VIII is about 1.8 times the value for the (orientationally disordered) ice VII. The structure of these two ices consists of two interpenetrating cubic lattices and it is not certain how τ_s in Eq. (2) is changed by interpenetration of two independently hydrogen-bonded lattices. Moreover, the lowest density, ambient pressure phases: ices Ih, XI and Ic have a higher value of κ than most of the other high-pressure (high-density) ices. It is apparent that these ambient pressure ice phases, whose structure contains linear hydrogen bonds with a tetrahedral angle between the neighbouring oxygen atoms have a highest mean free path or lowest scattering of phonons, and hence the highest κ. Only, ices VII and VIII at 2.4 GPa pressure, which are much denser have a higher value for κ.

In the crystal structure of the ambient pressure ice clathrates, hydrogen bonds are non-linear and the angle between the neighbouring oxygen atoms varies considerably for different water molecules [11]. In addition, the symmetrical cage-like structures formed by H_2O molecules in the clathrate structures contain small inorganic and organic molecules. These guest molecules neither lie exactly at the centre of the cage nor have the same orientation from one cage to the other. Thus the guest molecules in the clathrate structures have a long-range order neither for their molecular positions nor for their orientations. But at low temperatures, long range orientational order of tetrahydrofuran (THF) molecules inside the cages of the ice clathrate has been detected by dielectric measurements by Davidson [11], who surmised on this clathrate's potential for polarization-cooling in the same manner as magnetic cooling. This ordering has been studied in detail by Suga et al., by using calorimetry [66]. Even at high temperatures these clathrates have a much lower κ than the ices and a remarkably different variation of its value with temperature. Briefly, in contrast with crystals, whose κ decreases with increase in the temperature, κ of ice clathrates increases, as is seen in Fig. 3. Thus, in their κ against temperature behaviour, they mimic glasses and other amorphous solids and not the crystalline ices. The plot of κ against temperature for the ice clathrate, containing tetrahydrofuran (THF) as guest molecules, 17 H_2O-THF and 1.8×10^{-4}:1 molar ratio of KOH:H_2O [67,68] in Fig. 3, are shown in curve (a) for the low temperature orientationally ordered and in curve (b) for the high temperature orientationally disordered phases that x is negative, equal to -0.60 and -0.24 for the low and high temperature phases, respectively. The ~15% difference between κ of the two phases was attributed to proton-ordering, which seems to decrease the scattering rate slightly, possibly through a decrease in the anharmonicity [67]. A similar change in the magnitude of κ has been observed at the temperatures of ices Ih to XI transition where κ increases by ~20%, but without a significant change in x. This may also be explained in terms of decrease in anharmonicity [48] on orientational ordering of ice Ih.

Amongst the ice clathrates containing different guest molecules in their cage-like structures, κ changes by a relatively small amount when the guest molecules are changed in the same crystal structure of the clathrate [61,62,68]. This indicates that, as for an amorphous structure, phonon propagation distance becomes also strongly limited in the ice clathrates. This glass-like behaviour of the (crystalline) clathrates has been explained by using a resonance scattering model [69,70], according to which interactions between the encaged molecules and phonons cause strong phonon scattering. It is worth noting that the glass-like phonon scattering of a crystal was originally observed in 1981 by Ross et al. [71]. It is now being used [72] to obtain thermoelectric materials [64] with improved characteristics for use in technology.

We now discuss the magnitude of κ of the pressure-amorphized solid water, HDA. In our study, this solid was produced by very slowly pressurizing ices Ih and Ic at 130 K and taking several hours to reach 1.2 GPa. This is in contrast to the HDA made by rapidly pressurizing ices Ih and Ic at 77 K to 1.5 GPa in a few minutes. Since the pressure-amorphization is both pressure and time-dependent [73], and reaches completion more quickly at higher temperatures, the amorph produced by slow pressurization of ice Ih at 130 K in our study is likely to be the ultimate state of the high-density amorph. This aspect is to be stressed because there is a confusion regarding the identity of various "HDAs" that had been produced by pressurizing ice Ih at different temperatures to different pressures over a relatively short and often unspecified time period. Moreover, an ultimate, presumably highest density "HDA" seems to have been produced when the amorphous solid formed by

pressurizing ice Ih at 77 K was heated to 160 K while under a pressure greater than 0.8 GPa [74]. The plots in Fig. 3 show that amongst the solid forms of pure water, κ is lowest for the highest density HDA produced in our experiments. The lower κ value of a disordered solid is generally attributed to the lack of long-range propagating phonons, at least for high-frequency excitations, and this is likely to be the case for this HDA. Its κ increases with the temperature, as for most glasses and amorphous or structurally disordered solids, but the increase is less pronounced, as is indicated by its lower value of the quantity $x \sim -0.03$, than is normally found for glasses, of which amorphous SiO_2 is a well-known example [75]. (Note that SiO_2 has a high Debye temperature, which should be taken into account in a discussion of "weak" or "strong" dependence of κ on temperature.)

Although Eq. (2) had been derived for an ideal crystalline solid, we use it here to interpret qualitatively the change of κ as the structure of a material changes from crystalline to amorphous, as occurs on pressure-amorphization of ices Ih and Ic. To do so, we consider the grain boundary scattering time τ_{bs} which is written as, $\tau_{bs} = \ell/v$, where ℓ is the inter-grain distance or the linear dimension of the crystal [63]. Since the characteristic times for various scattering processes are assumed to be independent of each other, the resulting scattering time is obtained by the sum: $\tau_s^{-1} = \tau_{bs}^{-1} + \tau_{Ums}^{-1}$ for the boundary and for the Umklapp scattering denoted by τ_{bs} and τ_{Ums}, respectively. One reasonable approach thus is to consider that the solid formed by pressure-amorphization of a crystal has a vanishingly small crystal size. In this approach, as the size of crystals decreases, τ_s becomes smaller and finally reaches a temperature-independent, limiting value. In that case, τ_{Ums}^{-1} can be neglected in comparison with the large τ_{bs}^{-1} value and hence κ would be determined by ρ, C and v in Eq. (2). The quantities ρ, C and v vary with the temperature but much less than τ_s. To elaborate, at temperatures near the Debye temperature, C increases slowly with increase in the temperature, whereas the phonon velocity decreases, and thus the two partially compensate. In this respect, the relatively small increase in κ with increase in the temperature indicates that increase in C of HDA with increasing temperature is only slightly more than the concurrent decrease in the phonon velocity.

Thermal conductivity of the low-density amorph, LDA, which has been produced by heating HDA at ambient pressure or at $p < 0.07$ GPa, is also plotted against the temperature in Fig. 3. It shows that κ decreases with increase in the temperature. This is inconsistent with the generally held view that a roughly constant, or even slightly increasing κ with increasing temperature is a characteristic of a disordered solid and a strongly decreasing κ with increasing temperature is a characteristic of a crystal. It is also remarkable that as far as the temperature dependence of κ is concerned, HDA behaves like an amorphous solid and LDA behaves like a crystal [50]. For comparison, κ of vapour-deposited amorphous solid water has been calculated by Yu and Leitner [76], who used the term "glassy water", and by Klinger [77] by using molecular dynamics simulations and Eq. (2) and a pre-factor of 1/4 instead of 1/3. Both approaches have yielded κ values slightly higher than 0.2 $W\,m^{-1}\,K^{-1}$ at 100 K. More distinctively, the calculations have shown that κ increases with increasing temperature, opposite of that found for LDA.

Thermal conductivity of LDA is distinguished from that of other amorphous solids in one more aspect. Not only it varies according to, $\kappa \sim T^{-x}$ with x being close to 0.6, as for a crystal, but also its κ decreases with increase in pressure. This feature has been observed for a very few crystalline phases and for ices Ih and Ic, but not for an amorphous solid. At first sight, it seems that the mechanism that determines κ of LDA has a close relation with the mechanism that determines κ of ices Ih and Ic, particularly in view of the fact that the density [28] of the three solids is the same, and their specific heat [78,79] has been found to differ only by a small amount, if any. The effect of the proton- or hydrogen-atom disorder on κ has been evident from the observed increase by ~20% in κ when hydrogen atoms in ice Ih become partially ordered to produce ice XI, but the temperature dependence remains approximately the same on hydrogen-atom ordering, as seen in Fig. 3. In going from LDA to ices Ih or Ic, the hydrogen-atom disorder is maintained while the oxygen atoms become ordered and κ increases by a factor of 6–7, but the qualitative dependence of κ upon the temperature or pressure does not change. Such a similarity between LDA and ice Ic has also been observed from inelastic incoherent neutron scattering [80,81] and inelastic X-ray scattering [82] studies, which indicates phonon propagation up to unusually high frequencies, as is generally found for crystals. It also seems significant to consider here whether or not there is continuity between κ of LDA and that of liquid water in a temperature plane. In Fig. 3, the plot for κ of liquid water against temperature shows that, as for a disordered solid, it has a positive slope, and that this plot is not continuous with the plot for LDA, which has a negative slope. This seems to be a further demonstration that LDA is not a solid that would be obtained by cooling water at ambient pressure.

It is already known that thermodynamic properties of LDA differ from those of vapour-deposited amorphous solid and glassy water [83]. The lack of continuity between κ of LDA and ambient water in a temperature plane and the known thermodynamic differences between LDA and glassy water [83] provide additional evidence against the validity of the two-liquid model of water [44], which had assumed that ambient pressure water is a liquid counterpart of solid LDA.

3.2. Heat capacity of water's high-density amorph

To complete this section we now discuss the C_p of HDA. It increases with increase in the pressure, which increases the density. This is particularly significant because HDA at a fixed $p > 0.5$ GPa has also been found to become gradually denser on heating from 77 K, and then to explosively crystallize at ~160 K when p is ~1 GPa [74,84]. Increase in pressure on water's amorphous solids may cause both the oxygen–oxygen distances and the O–H–O angles in its structure to change by distorting the structure differently in different parts of bulk phase. This change would differ from the manner in which increase in pressure causes the distances and angles in the crystalline ices to change without distorting the structure. It is generally known

that C_p of a solid decreases with increase in the density and, although it has not been measured for the high pressure forms of the ices, experiments have shown that the frequency of translational lattice vibrations of all high pressure ices, including ice VI (at pressures of the high-density amorphous ice formation) increases as the density increases with increase in the pressure [85]. The origin for the observed decrease in C_p with increase in pressure and density has consequences for the recent finding that some of the vibrational features of HDA, as studied by neutron scattering, are crystal-like [86]. In relevance to the structure of HDA, these findings need to be interpreted together with the above-mentioned changes observed in C_p of the ices.

The measured κ of the HDA at 130 K is plotted against the pressure in Fig. 4(A). The plot shows an asymptotic increase with pressure, which is well described by the equation: $\kappa = 0.5856 + 0.1708p - 0.0781p^2$. The anharmonic part of C_p that is associated with the thermal expansion is given by the relation, $C_p - C_v = TV\alpha^2/\beta$, where V is the molar volume, α the volume thermal expansion coefficient and β is the isothermal compressibility. The quantity $C_p - C_v$ has been estimated as $\sim$0.025 J mol^{-1} K^{-1} at 100 K [87]. By using $V = 15.4 \times 10^{-6}$ m^3 mol^{-1} [27], $\beta = 0.10$ GPa^{-1} [32], and α of HDA equal to that for ice Ih at 100 K ($\alpha = 3 \times 10^{-5}$ K^{-1}) [88], we determine the term $TV\alpha^2/\beta$ as $\sim$0.015 J mol^{-1} K^{-1}, which seems negligible in comparison with its C_p of $\sim$23 J mol^{-1} K^{-1} [35].

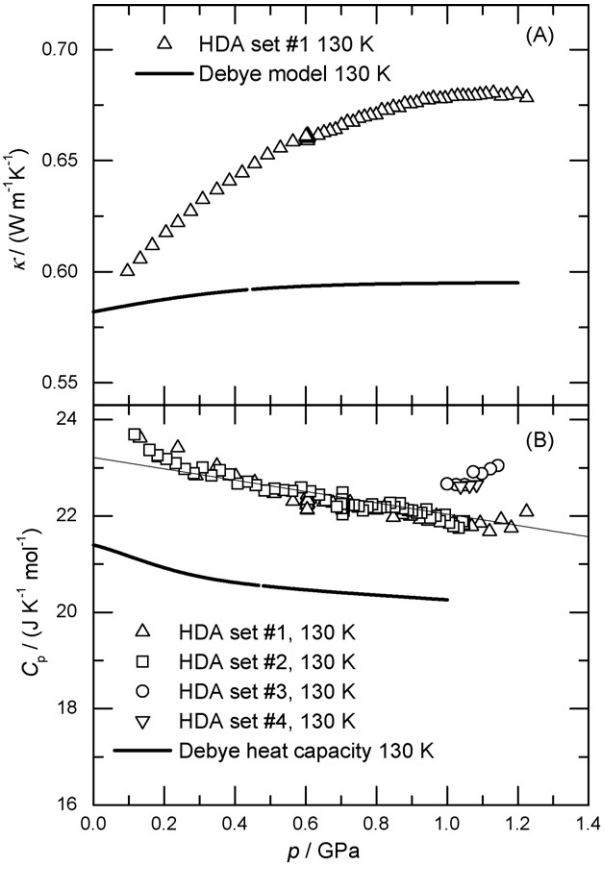

Fig. 4. (A) Typical plots of the thermal conductivity of the amorph measured at 130 K against the pressure. (B) The specific heat per mole of water's high-density amorph (HDA) measured at 130 K is plotted against the pressure. The notations refer to different runs in which each time a new sample of the amorph had been prepared and studied. Smooth curves show the calculations based on the Debye model for thermal conductivity and heat capacity. Data are taken from Ref. [35].

The C_p of HDA at 130 K measured as a function of pressure is plotted in Fig. 4(B). The plot shows that C_p decreases asymptotically as the volume decreases when the pressure is increased. But its value is not expected to become constant at very high pressures because compressibility, a measure of decrease in volume, does not become zero at high pressures. The decrease in C_p with increase in pressure for solids, or a negative value of $(\partial C_p/\partial p)_T$, indicates that the phonon frequency increases with increase in pressure. It is thermodynamically related to the thermal expansion by $(\partial C_p/\partial p)_T = -T(\partial^2 V/\partial T^2)_p$. Since the thermal expansion coefficient, $\alpha = V^{-1}(\partial V/\partial T)_p$, a negative value of $(\partial C_p/\partial p)_T$ indicates that α increases as T increases. This indicates that the α-determining Grüneisen parameter would have a positive value and, consequently, a decrease in V with increase in p increases the frequency of the phonon modes. In a recent study, we have deduced that the average for the low-frequency Grüneisen parameters is positive for HDA but negative for ice Ih [89].

The Debye model has also been used to estimate how κ and C_v vary with the pressure. This is done by calculating the Debye temperature, $\theta_D = v\bar{h}/k_B(6\pi^2\rho/M)^{1/3}$ where v is the average sound velocity, which increases from 2300 m s^{-1} at atmospheric pressure to 2600 m s^{-1} at 1 GPa pressure [32,35], and M is the mass of the vibrating unit, taken as the molecular weight [35]. The Debye temperature was found to increase from 230 K at 0.01 MPa to 271 K at 1 GPa, which corresponds to a decrease in C_v by $\sim$1.1 J mol^{-1} K^{-1}. For comparison, we note that the Debye temperature of ice Ih is 220 K at atmospheric pressure [90]. Since this decrease is $\sim$2% less than the decrease in C_p for an equally large pressure increase [35], and since the $TV\alpha^2/\beta$ term is negligibly small, the measured decrease in C_p agrees with the calculated decrease in C_v, within the measurement and analytical errors. This shows that increase in the frequency of the phonon modes with increase in pressure can account for the decrease in C_p of HDA. Hence, we conclude that an increase in pressure does not greatly affect the anharmonic part of C_p.

In the theoretical details of the Debye model for the frequency dependence of phonon scattering, Eq. (2) for κ is written as [63]

$$\kappa = \frac{k_B^4 T^3}{2v\pi^2\bar{h}^3} \int_0^{\theta_D/T} \tau(x) \frac{x^4 e^x}{(e^x - 1)^2} \, dx \qquad (3)$$

where v is the phonon velocity, $\tau(x)$ the resultant relaxation time and $x = \bar{h}\omega/k_B T$ with ω being the phonon angular frequency. We used an earlier finding of phonon-like excitations in the HDA [86] extending up to high frequencies and evaluated κ by using Eq. (3). Its value, which is plotted against p as a continuous line in Fig. 4(A), is significantly less than the measured κ, but the plot is qualitatively similar to that of the measured κ. The rate of increase ($d\kappa/dp$) is however much smaller than that observed experimentally, which may indicate a change in the scattering strength with increase in pressure.

The results for HDA at 130 K, shown in Fig. 4(A) and (B), refer to the state of a solid produced by a much slower isothermal pressurization of ice Ih at 130 K than has been used to produce HDA in all other studies, and it is therefore denser than the state obtained by pressurizing at 77 K. As a consequence, the properties such as κ, C_p, v and θ_D would also be somewhat different. For example, its Debye temperature and sound velocity would be higher than that of HDA produced by the usually rapid pressurization at 77 K. The difference in density itself could have a large effect on some properties, and must therefore be taken into account in a discussion of HDAs properties by appropriately describing the sample's preparation and history. As shown in Fig. 4(A) and (B), κ and C_p of the sample do not vary strongly with pressure (and density). However, the ultimate dense form of HDA should have a lower C_p and higher κ than the samples of HDA produced by rapid pressurization at 77 K. Moreover, the pressure-induced changes in κ and C_p would be slightly less pronounced as the compressibility would be smaller for the denser forms of HDA and lowest for the ultimate or the densest form.

On the basis of the preceding analysis, we conclude that when the internal energy of HDA is increased by increasing the pressure, the frequency of phonon modes increases and the Debye energy and the anharmonicity decrease. While the Debye phonons can explain the decrease in C_p of HDA by ∼5% per GPa, and also the increase in κ towards a plateau value, they do not quantitatively describe the increase in κ within the approximation of a constant phonon scattering strength. Its quantitative description would require that a term for pressure-dependent scattering strength, which would be consistent with the pressure-induced decrease of the anharmonicity, and/or a term for other pressure-dependent processes be included.

4. Relaxation properties of the amorph and conversion to ultraviscous water

Consequences of molecular self-diffusion that allows a solid or a liquid to explore different configurations are usually determined by calorimetry and dielectric spectroscopy. Differential scanning calorimetry yields a glass transition temperature, T_g, which is taken as either the onset of the sigmoid-shape rise in the heat flow signal (or equivalently C_p) for a given heating rate, or occasionally as the mid-temperature of the sigmoid-shape rise. Dielectric spectroscopy yields the relaxation time of the ultraviscous liquid formed on heating the glassy state. For materials, whose vitreous state rapidly crystallizes on heating, the endotherm is not clearly observed and alternative procedures have been used for determining whether or not they are truly amorphous, particularly when diffraction methods are unable to distinguish an amorphous solid from a microcrystalline solid. Discussion of this subject has been provided in an earlier paper in relevance to the majority of hyperquenched metal-alloys, glassy water, and amorphous solid state of low molecular weight hydrocarbons [91]. In the following sections we first describe how the various amorphous solid waters are produced, and then how their relaxational properties change with temperature.

4.1. Preparation of water's amorphous solid and glassy states

It is well known that water does not supercool easily to form a vitreous solid. Therefore its amorphous solids have been prepared in different ways. Briefly, vapour-deposited amorphous solid water (ASW) is made by slow deposition of water vapours on a few millimeter thick copper plate kept at a temperature below 100 K. This copper plate is held by screws in close contact with another copper plate that forms the bottom of a 6–8 cm diameter glass tube containing liquid nitrogen. The other end of the glass tube is kept open to atmosphere for replenishing with liquid nitrogen. In this home-made assembly, vacuum is maintained and the path of vapours from water contained in a flask is interrupted by a baffle. Thus only a fraction of the amount of vapours is allowed to deposit on the copper plate. After sufficient deposition in a period of 3–4 h, the vacuum is released, the glass tube containing liquid nitrogen is taken out of the vacuum assembly, and quickly immersed in a bath of liquid nitrogen. The ASW sample is then dislodged from the copper plate into a liquid nitrogen bath by using a scraper, and thereafter all handling of the sample is done by using thermally insulated tools with the sample immersed in the liquid nitrogen bath. Hyperquenched glassy water (HGW) is also made by using a home-built assembly. In its preparation, pure water droplets are produced by means of an ultrasonic nebulizer and dispersed as an aerosol in nitrogen gas. The aerosol is confined to a large glass tube and the droplets are then allowed to enter a high vacuum cryostat through a 200 or 300 μm aperture. The droplets that enter into the vacuum assembly through this aperture gain a supersonic speed and hit a 35 mm diameter 4 mm thick copper plate kept at ∼77 K. This copper plate is mounted at the end of a flat bottom tube containing liquid nitrogen whose one end is open to the atmosphere for replenishing it with liquid nitrogen. The droplets thus splat on the surface of the copper plate and cool at a rate higher than 10^5 K s^{-1}. After several hours, a porcelain-like, 2–3 mm thick layer of HGW is thus obtained. Details of the procedure are given in Refs. [23–25] and micrographs of the rather irregular shape of the splat-cooled droplets of HGW have appeared in Refs. [92,93]. The procedures for recovering HGW sample and its handling in a liquid nitrogen bath are the same as described above for ASW.

Preparation and recovery of HDA and LDA are less tedious. HDA is made by first freezing water at ambient pressure inside a piston cylinder assembly kept immersed in liquid nitrogen and then uniaxially compressing the ice Ih formed isothermally at ∼77 K to ∼1.5 GPa, or else (nonisothermally) at temperatures below 130 K to ∼1.5 GPa. As mentioned earlier here the HDAs produced in this manner differ in properties depending upon the temperature pressure and time profiles used in the preparation. The HDA sample is depressurized to ambient pressure at a low temperature and then extracted from the piston-cylinder assembly by pushing it out of the cylinder into liquid nitrogen. LDA is produced by heating HDA to a temperature range of 115–130 K at ambient pressure [28] or at a pressure below 0.07 GPa [34,50]. Water's amorphous solids are produced by two more methods: one is by irradiation of ice Ih at low tem-

peratures by high energy photons or other particles [94–96] and second is by decompression of ice VII to ambient pressure at 77 K and heating to T > 120 K, which produces LDA [97].

4.2. Calorimetric behaviour, relaxation and glass-softening

Ambient pressure differential scanning calorimetry studies have shown that the enthalpy of both ASW and HGW decreases on isothermal annealing in vacuum for several hours, as discussed earlier [26]. In the case of ASW the surface area rapidly decreases and as sintering proceeds any pores in it become closed and isolated from each other. When the initial heating is carried out in the presence of N_2 or other gases, the adsorbed gases become enclosed in the pores during sintering. Once enclosed in the pores the gases cannot be removed by pumping at low temperatures but are released when the sample is gradually warmed up to 273 K. This release of gases causes the appearance of additional features in the DSC scans which become further modified by the different thermal conductivities of the gas that is used as purge gas. To minimize the exothermic effects due to reduction of surface area on initial heating, ASW samples are first heated in vacuum up to 113 K, which decreases the surface area by several hundred $m^2\,g^{-1}$ and no gas is enclosed in the pores during the sintering of the micro-porous solid [26]. Annealing at higher temperature or slow heating to higher temperatures causes weakly hydrogen-bonded water molecules to become mobile and any dangling OH groups in the structure to form hydrogen bonds with the neighbouring molecules' oxygen atoms. This occurs in addition to the structural relaxation that densifies a vapour-deposited amorphous solid and reduces its fictive temperature, T_f, the temperature at which the glass and the equilibrium liquid would have the same thermodynamic properties. Annealing or slow heating of HGW decreases its enthalpy almost entirely as a result of structural relaxation and reduces its T_f with time.

Until 1987, all attempts to detect the glass-softening endotherm for ASW and HGW had been unsuccessful, because the samples rapidly crystallized to ice Ic even when heated at a high rate in a DSC experiment [98], and it was puzzling how use of adiabatic calorimetry in an earlier study [99] could have shown an (endothermic) rise in C_p of ASW by $\sim$35 $J\,mol^{-1}\,K^{-1}$ at a temperature of 135 K. Further DSC studies showed [26,98,100] that there were two partly overlapping exotherms in the differential scanning calorimetry (DSC) heating scans for both ASW and HGW. The low temperature exotherm was due to structural relaxation of the solid and the high temperature and deeper exotherm was due to the rapid crystallization of the ultraviscous water, formed on heating ASW and HGW, to ice Ic. It appeared that part of the heat released on structural relaxation could cause ASW and HGW to rapidly crystallize in the glass-softening endotherm region. Therefore, it was deduced that a procedure that eliminated the relatively large exotherm during the scanning could help reveal the glass-softening endotherm in a DSC scan. This led to development of an anneal-and-scan procedure for determining T_g of ASW, HGW [25,26] and hyperquenched metal alloy glasses [91,101]. In this procedure, the sample is first annealed at a certain temperature for a period long enough to allow its structural relaxation and to lose its relatively high enthalpy, then cooled to a lower temperature and finally heated to obtain its DSC scan. As a result, the enthalpy release on structural relaxation during heating is negligibly small, and therefore does not interfere with the appearance of the T_g endotherm. The procedure has been useful for determining T_g of materials that cannot be vitrified by the normal method of cooling at a rate of up to 100 $K\,s^{-1}$, and whose vitreous state once produced rapidly crystallizes on heating prior to showing a T_g endotherm in a normal DSC scan [91,101], as well as for determining whether a solid is microcrystalline or amorphous, particularly when diffraction methods are unable to do so [101].

A detailed discussion of the entropy and enthalpy of ASW, HGW, HDA and LDA has appeared in Ref. [102], where the temperature dependence of their enthalpy and the irreversible but cyclic thermodynamic paths and crystallization have been discussed. As mentioned above, a quantitative comparison of the properties of ASW, HGW and LDA must take into account the heat effects resulting from their spontaneous relaxation. Nevertheless, to describe some of these features briefly here, the DSC scans of ASW, HGW and LDA obtained by heating at 30 $K\,min^{-1}$ rate are shown in Fig. 5(A). The top two plots show the scans for the as-made samples of ASW and HGW. The initial, broad exotherm observed for ASW is due to the release of enthalpy on reduction in the surface area as well as due to structural relaxation. This exotherm is much less pronounced for HGW in which only enthalpy relaxation occurs. The deep exothermic feature with a minimum at T near 160 K is due to crystallization of ASW and of HGW to ice Ic. After the onset of crystallization, the exotherm for HGW has a slightly lesser slope than for ASW, as if there are two steps involved in crystallization of HGW. It has been speculated that this may be related to the anomalous behaviour of supercooled liquid water, but its reason is not understood [26,103]. The samples discussed in Ref. [102] were then structurally relaxed by annealing at a temperature below their crystallization onset temperature or else by heating to a temperature just below their crystallization onset, cooling and then reheating to obtain a DSC scan. The arrows in the plots show their T_g. Its value is 136 ± 1 K for ASW and HGW [26] and 129 ± 1 K for LDA for the heating rate of 30 $K\,min^{-1}$ [104]. The increase in C_p is 1.6 $J\,mol^{-1}\,K^{-1}$ for ASW and HGW and 2.0 $J\,mol^{-1}\,K^{-1}$ for LDA [104]. This increase occurs over an unusually broad temperature range, which indicates an exceptionally large distribution of relaxation times and, as discussed earlier [105,106], a low value for the relaxation's nonlinearity parameter. Moreover, the relatively small increase in C_p in the glass-transition range has been interpreted in terms of a small rate of entropy change of a state whose configurational entropy is already small [107]. Further studies of the hyperquenched glassy states of dilute solutions of inorganic and organic substances showed that T_g varies with both the nature of impurities and their concentration [108,109] in the glassy state and that T_g shows a minimum value for a certain concentration.

We recall that like all physical properties, the enthalpy of ASW, HGW, HDA and also of LDA depends on the sample history and, therefore, is not likely to be the same for samples of

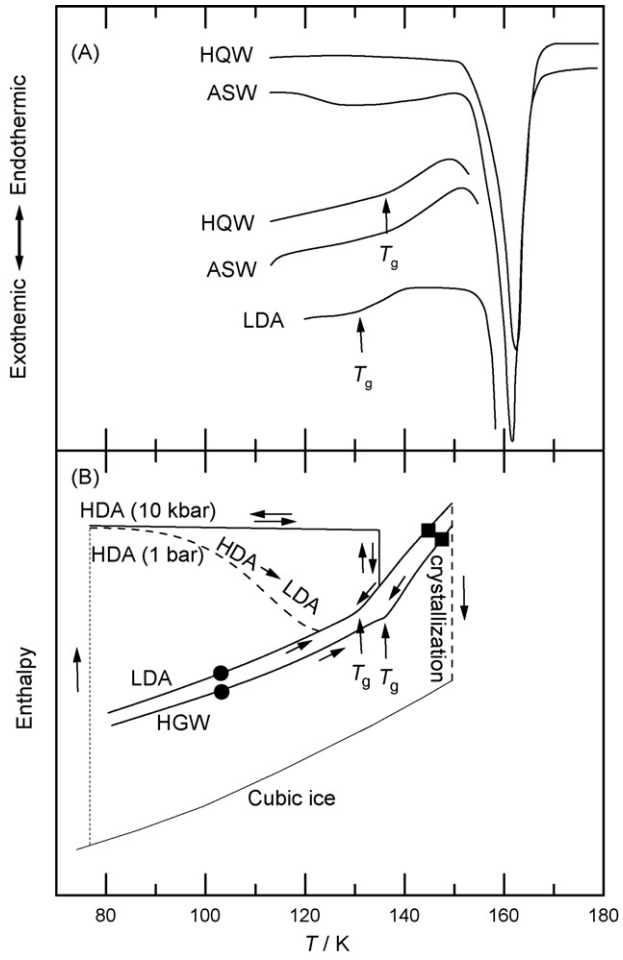

Fig. 5. (A) DSC scans showing the glass–liquid transition endotherms and crystallization exotherms for vapour-deposited amorphous solid water (ASW), hyperquenched glassy water (HGW) and low-density amorph (LDA). The T_g endotherm is masked by the heat released on enthalpy relaxation and surface area decrease in the top two curves, which also show sharp crystallization exotherms. The bottom three show the glass–liquid transition endotherms with T_g marked by the arrow. (B) An illustration for the temperature dependence of the enthalpy of ASW, HGW and LDA. The T_g s are 136 ± 1 K for ASW and HGW and 129 ± 1 K for LDA, and the increase in C_p is $1.6\,J\,mol^{-1}\,K^{-1}$ for ASW and HGW and $2\,J\,mol^{-1}\,K^{-1}$ for LDA. Arrows show the direction of transformation (two arrows opposite in direction denote the reversibility of the path). The temperature and pressure conditions are marked, and the notation for the paths is described in the text. The plots for the enthalpy are drawn such as to show the measured magnitude of q_{irrev} for HDA → LDA, LDA → ice Ic and HGW → ice Ic transformations. The vertical axis has no scale because the absolute value of the enthalpy is not known. The data are replots from Figs. 2 and 3 of Ref. [102].

different thermal and pressure histories. In the cases of ASW and HGW, the rapid cooling rate necessary to avoid crystallization to ices Ih or Ic inevitably produces a high-enthalpy state, which relaxes to a lower-enthalpy disordered state on annealing at T slightly below T_g. In the case of HDA, a high-enthalpy state is formed on pressurization of ices Ih or Ic at 77 K, and it relaxes to a lower-enthalpy state on heating at a fixed pressure of e.g. ∼1 GPa to T above 130 K. Consequently, the exact manner in which the enthalpy varies with T on heating at ∼1 GPa depends on the heating rate. In terms of the enthalpy, lowering of the temperature for producing HDA by isothermally pressurizing ices Ih and Ic is analogous to increasing the cooling rate for producing the glassy state at a fixed pressure. Nevertheless, we have shown the variation of the enthalpy of HDA, LDA, ASW, HGW and ice Ic over the temperature range of interest in Fig. 5(B), where the respective T_gs have been indicated. Here, the change in slope at T_g has been made consistent with the relative change in C_p of the amorphs, and the manners of irreversible transformation from ices Ih and Ic to HDA on compression to 1 GPa has been indicated. Also, the irreversible path for HDAs conversion to LDA, the LDAs glass–liquid transition and finally the crystallization to ice Ic have all been indicated by arrows. It is shown that the cyclic path for ice Ic *via* HDA and LDA has three irreversible transformations, (i) from ice Ic to HDA, (ii) from HDA to LDA and (iii) from the high temperature state of LDA to ice Ic.

It should be stressed that in Fig. 5B, the paths of LDA and HGW (and ASW) follow different enthalpy–temperature curves, and these curves do not meet. This means that the hydrogen bond network structure of LDA at T above its T_g of 129 K does not convert on heating or cooling to the hydrogen bond network structure of HGW. Also, the hydrogen bond network structure of ultraviscous water formed on heating HGW does not convert on cooling to the hydrogen bond network structure of LDA. We infer that there is a difference between the short-range order, not necessarily limited to first near neighbours in the structures of LDA and HGW. Similar differences have been indicated by the thermal conductivity data of LDA [50], whose temperature dependence is more like that of a crystalline than of an amorphous solid. More recently this difference is also found from dielectric relaxation measurements of LDA [110].

Studies of deuterated LDA have shown that T_g increases from 129 K to ∼133 K on deuteration, an increase of 4 K, but ∼3–5 K for differently prepared samples [111], which is significantly higher than the increase of ∼1 K observed for the deuterated HGW [112]. This also indicates the difference between the diffusion kinetics of LDA from HGW. Further detailed studies of LDA have been performed by adding different impurities that dissolve in ice Ih and are incorporated in its lattice structure, and further by varying the impurity components such as to alter the rate of orientational diffusion of water molecules in LDA, as is known to occur in ice Ih [111]. Briefly, LDA made from ice Ih containing HF, NH_3 and NH_4F, which are expected to produce proton-deficient and proton-rich topologically disordered structures, have shown that the glass-softening endotherm for LDA containing HF becomes too broad to yield its T_g. The T_g of LDA containing NH_3 decreases to 127 K and of that containing NH_4F remains at 129 K. Since NH_3 in the hydrogen-bonded network structure increases the number of protons, and is hence seen to increase the dielectric relaxation time [113], it is expected that if orientational diffusion of H_2O molecules were to contribute to the increase in the number of configurations accessible to the LDA structure, T_g of the NH_3-doped LDA would be higher than 129 K, the value for pure LDA. For the same reason, introduction of NH_4F is seen not to introduce any extra protons in the hydrogen-bonded structure and therefore should not effect the dielectric relaxation time or, for the reason given above, LDAs T_g. The T_g of NH_4F-doped LDA does remains at 129 K [111]. Thus not only the thermodynamic vibrational and relaxational

properties of LDA differ from those of ASW and HGW, but also the effects of deuteration and impurities on their dynamics differ.

4.3. Dielectric relaxation of amorphous solid and glassy states of water

Initially dielectric loss factor measurements were performed on ASW [114] and HGW [115] in order to investigate if the relaxation time of its ultraviscous state could be determined in the same manner as for other glasses. But it was observed that the relatively slow rate of heating needed for such measurements always crystallized the sample to ice Ic and this crystallization also yielded a peak in the loss factor against temperature plots. Although dielectric measurements did not allow measurement of their crystallization kinetics to ice Ic, the crystallization kinetics of ASW made from H_2O and D_2O has been studied by both calorimetry and FTIR spectroscopy in real time [116,117]. It has been found that crystallization follows the Avrami equation and the activation energy for the crystallization is 51 kJ mol^{-1} for H_2O and 66 kJ mol^{-1} for D_2O with an uncertainty of ±10 kJ mol^{-1}. It has also been suggested that the exponent of the Avrami equation can be seen also to indicate a temperature-dependent activation energy or barrier height to the ASWs crystallization to ice Ic [116,117].

More recently, the measured change in the dielectric loss tangent, $\tan\delta$, of both ASW and HGW with temperature has been analysed in detail, and it has been shown that approximate value of the dielectric relaxation time of ultraviscous water can be estimated from an analysis of the data available at only two frequencies [118,119]. In this analysis, the measured value of the dielectric loss tangent, $\tan\delta_{\text{meas}}$ at two frequencies, ω_1 and ω_2, is given by

$$\frac{\tan\delta_{\text{meas}}(\omega_1) - \tan\delta_{\text{background}}}{\tan\delta_{\text{meas}}(\omega_2) - \tan\delta_{\text{background}}} = \left(\frac{\omega_2}{\omega_1}\right)^{\beta} \tag{4}$$

where $\tan\delta_{\text{background}}$ is the frequency-independent but temperature-dependent value of the dielectric loss which contributes to $\tan\delta_{\text{meas}}$, β the asymmetric distribution of relaxation time parameter of the Davidson–Cole equation [120] and the frequencies ω_1 and ω_2 are much greater than $1/\tau_{\text{diel}}$, where τ_{diel} is the dielectric relaxation time. For a reasonable choice of β, $\tan\delta_{\text{background}}$ can be determined from the tan δ_{meas} values measured at two frequencies. For the same $\omega^2\ \tau^2 \gg 1$ condition at a fixed temperature, the dielectric loss, ε'', and $\tan\delta_{\alpha\text{-relaxation}}(\omega) = [\tan\delta_{\text{meas}}(\omega) - \tan\delta_{\text{background}}]$ are related to τ_{diel} by

$$\varepsilon'' = \frac{\Delta\varepsilon}{(\omega\tau_{\text{diel}})^{\beta}}; \qquad \tau_{\text{diel}} = \frac{1}{\omega}\left(\frac{\Delta\varepsilon}{\varepsilon_\infty \tan\delta_{\alpha\text{-relaxation}}}\right)^{1/\beta} \tag{5}$$

where ε_∞ is the limiting high frequency permittivity. Since,

$$\omega_{\max}\tau_{\text{diel}} = \tan\left[\frac{\pi}{2(\beta+1)}\right], \tag{6}$$

$\omega_{\max}\tau_{\text{diel}} \neq 1$, in this distribution of relaxation times [120,121]. The dielectric relaxation time, τ_{diel}, therefore determined from Eq. (6), as described in detail earlier [119]. The dielectric relaxation time of ASW has thus been estimated as 23 s at 140 K and that of HGW as 35 s, with a factor of two uncertainty in both estimates [119]. This analysis, however, did not indicate the temperature dependence of the dielectric relaxation time of ultraviscous water.

Reorientational and translational diffusion motions of H_2O molecules in liquid water with tetrahedral hydrogen bonding require that hydrogen bond break and then reform with a new neighbour or the same neighbour. Therefore, thermally activated rotational and translational motions of molecules in disordered and predominantly network structures, such as those of ultraviscous water and molten SiO_2, occur together. Since the dielectric relaxation time, the self-diffusion time, and the structural relaxation time estimated from the T_g endotherm are usually found to differ by about one order of magnitude or less, the above given estimate of the dielectric relaxation time of ∼30 s clearly established that heating ASW and HGW to 140 K produces an ultraviscous state of water at 140 K, and their T_gs are 136 K for the 30 K min^{-1} heating rate.

In contrast, the dielectric relaxation time of HDA and LDA has been determined directly by measuring the dielectric permittivity and loss, ε' and ε'', spectra, as their states at high temperatures seem to be stable for long enough time to allow such measurements [53,54,110]. For this study, the HDA sample was made by amorphizing ice Ih at 130 K by raising the pressure to 1.2 GPa at a rate of 0.1 GPa h^{-1}, and then keeping the amorphized state near 1 GPa and 130 K for 1 h. The pressure on the amorph at 130 K was slowly decreased from 1.2 to 1 GPa and thereafter its dielectric relaxation spectra at 130 K was measured in the 0.01 Hz to 1 MHz range [53,54]. Typical spectra of the dielectric loss, ε'', for the pure and KOH-doped amorphized-ice at 1 GPa are shown in Fig. 6(A). These show that the ε'' peak moves to higher frequencies when HDAs temperature is increased, showing that the relaxation becomes faster. At a temperature near 150 K, the height of the ε'' peak begins to decrease, indicating that the sample has begun to crystallize and the process becomes faster on heating above 150 K. This also indicates that the solid formed on crystallization does not significantly contribute to ε'' in the frequency range of measurements, not necessarily that the orientation polarization of the state formed is less.

To confirm that crystallization occurred, the temperature difference between the sample and the Teflon vessel, ΔT was also determined simultaneously in the same experiment, and it is plotted against the sample's temperature in Fig. 6(B). It shows a small, slowly growing exothermic effect which reaches a local maximum at ∼150 K. Thus slow crystallization had begun at $T < 150$ and it accelerated at $T > 150$ K. It has been found already that on slow heating at a pressure of ∼1 GPa, the fully dense pressure-amorphized state crystallizes at T near 165 K [84]. In view of that, the temperature of one sample was decreased from 138 K to 132 K, which is well below the above-mentioned crystallization onset temperature and the ε'' spectra were measured again. The spectra measured at 132 K after this cooling was found to be identical to the spectra that had been measured at 132 K after heating the HDA sample to 132 K, confirming that

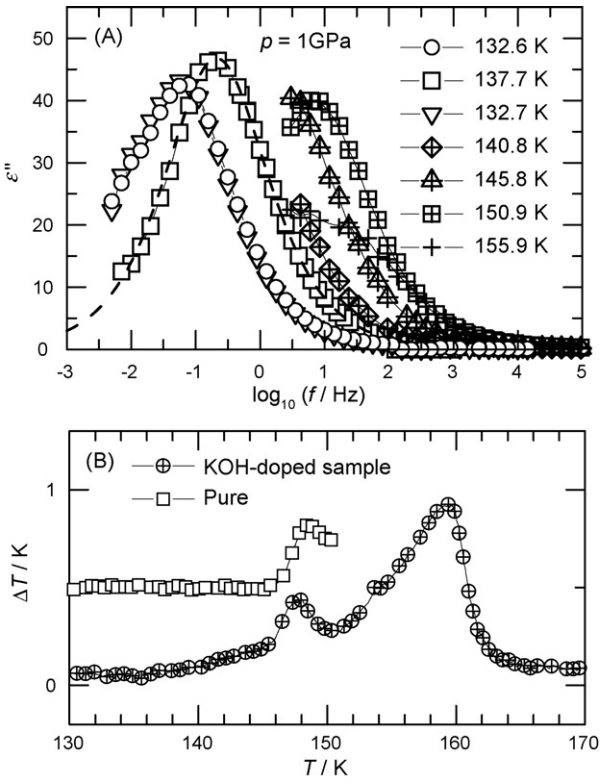

Fig. 6. (A) The dielectric loss spectra for pure amorph (open symbols) and KOH-doped amorph (symbols filled with a cross) at 1 GPa at the temperatures indicated, and an analysis in terms of the Cole–Cole symmetrical distribution of relaxation times (dashed line). (B) The temperature difference between the sample and the sample cell ΔT, as observed on heating of the pure HDA and 1.7×10^{-4} mole fraction KOH-doped HDA. A baseline has been subtracted from the data, and the curves have been shifted vertically for clarity. Data are taken from Refs. [53,54].

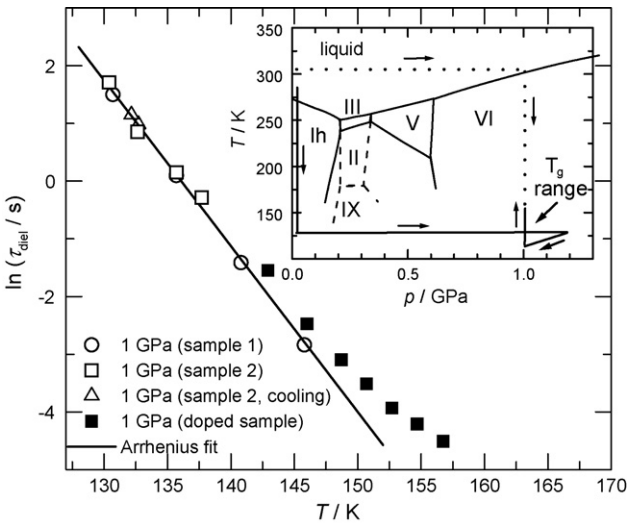

Fig. 7. The relaxation time of pure HDA at 1 GPa plotted against the temperature. The line is the best fit of the Arrhenius equation. Data are taken from Refs. [53,54]. Insert is the phase diagram of the ices. The temperature–pressure region in which amorphization studies of ice Ih have been performed is indicated. The path that leads to an ultraviscous liquid state is shown by arrows. The path from the liquid water to ultraviscous state shown by the dashed line requires supercooling at 1 GPa. This path has not been experimentally achieved.

the spectra did not change on thermal cycling. Therefore, we conclude that the HDA sample is thermodynamically in the fully relaxed state already at T close to 130 K.

As shown in Fig. 6(A), the ε'' spectra are described by a symmetrical distribution of relaxation times function given by the Cole and Cole [122]: $\varepsilon^*(\omega) = \varepsilon_\infty + (\varepsilon_0 - \varepsilon_\infty)/[1+(i\omega\tau_{diel})^{1-\alpha}]$, where ω (=$2\pi f$) is the angular frequency and τ_{diel} is the characteristic dielectric relaxation time. (Note that this type of distribution has been found for water also in the range 273–323 K [123]. For a detailed discussion see Ref. [54].) The τ_{diel} value was calculated from the reciprocal of the peak frequency in the ε'' spectrum, i.e., $\tau_{diel} = (2\pi f_{peak})^{-1}$, and it is plotted against the temperature in Fig. 7. At 150 K, τ_{diel} is 30 ± 5 ms for both pure and KOH-doped water, which shows that this amount of doping has no discernible effect on τ_{diel} of HDA at 1 GPa, although it has a very large effect on the relaxation of time of ice Ih [124]. These findings are consistent with the general observation that the relaxation time of liquid water is not greatly affected by the addition of small amounts of electrolytes.

The temperature dependence of τ_{diel} is described well by the Arrhenius relation, i.e., $\log_{10}(\tau_{diel})$ varies linearly with $1/T$, as is shown by the solid line in Fig. 7. The relaxation time is 5 s at 130 K and 30 ms at 150 K, which is surprisingly shorter that τ_{diel} of HGW and ASW, which has been estimated as 30 s at 140 K and ambient pressure. Moreover, τ_{diel} at 130 K is significantly shorter than 100 s to 1 ks, a value normally taken to be the calorimetric relaxation time at T_g of glass-forming liquids. These results therefore indicate that HDA at 1 GPa becomes an ultraviscous liquid well before it crystallizes on heating to 150 K.

In this context, it is noteworthy that τ_{diel} of LDA [110] has been found to be longer than that of HDA by more than a factor of 10, despite the fact that its density is ∼25% less than that of HDA which should decrease τ_{diel}. More significantly τ_{diel} of LDA is in between that of HDA and ice Ic [110]. Now, it is known that among the different states of water, τ_{diel} of the state with a fully bonded hydrogen-bonded structure, with hydrogen atom distributed according to the ice rules is longer than τ_{diel} of a structure that does not obey the ice rules, as is known from a comparison of τ_{diel} of ice Ih and that of liquid water. (The ice rules are that there are two hydrogen atoms adjacent to each oxygen atom, and there is only one hydrogen atom per hydrogen bond.) By analogy, therefore, the higher τ_{diel} value for LDA relative to that of HDA would indicate formation of a hydrogen bond structure in LDA in which the ice rules are obeyed. Thus HDA may appear to be a densified state of water in which ice rules are not obeyed. It is possible that the crystal-like temperature dependence of thermal conductivity of LDA is a reflection of its structure in which there are two hydrogen atoms adjacent to each oxygen atom, and there is only one hydrogen atom per hydrogen bond, as is the case for thermal conductivity for all the crystalline ices whose κ value is plotted in Fig. 3. Therefore, the decrease in the density on the irreversible transformation of HDA to LDA is also accompanied by a change in the manner of hydrogen bonding from that in water to that in the crystalline ices.

We conclude that τ_{diel} of 30 ± 5 ms for HDA at 150 K shows that it becomes an ultraviscous high-density liquid on heating.

It is in an equilibrium but metastable state, the one that would be obtained by supercooling water at a pressure of 1 GPa across its phase boundary with ice VI, which is shown in the phase diagram in Fig. 1, and discussed later here. Since LDA is not thermodynamically connected to the (low-density) water obtained by heating ASW and HGW [83], it seems that it does not form the (low-density) water on heating. This is also evident from the finding of the crystal-like variation of its thermal conductivity with temperature as shown in Fig. 3, from the analysis of the inelastic neutron scattering data [80,81] and inelastic X-ray scattering data [82] and from the thermodynamic, vibrational and T_g-related properties [37,83,110–112], as discussed earlier here. Thus it does not seem that the low-density liquid water is related to LDA. This puts into question the conjecture of HDA–LDA equilibrium and the transition between their corresponding liquid states, in particular the conjecture that HDA and LDA may be vitrified states of two distinct liquid states of water whose densities differ by ∼25% [44].

It should be noted that a DSC feature resembling the T_g-endotherm of the type observed for ASW, HGW and LDA shown in Fig. 5(A) has also been observed in the calorimetric studies of purposely aged samples of ice Ic [107,125], ices V and VI [126,127] and of tetrahydrofuran-ice clathrate [107,128]. During the ageing at a low temperature, these crystalline solids undergo proton-ordering, which should be an exothermic process. When the obtained partially proton-ordered state is heated, it gains enthalpy in a time-, and temperature-dependent manner and the DSC scan shows a peak whose area is equivalent to the enthalpy lost on annealing. An estimate for the extent of orientational- or proton-ordering in the ices has been obtained from the measured gain in enthalpy on heating. But in the case of ASW and HGW, unannealed samples have shown the T_g-endotherm on thermal cycling over a limited temperature range, and isothermally annealed samples for different periods have shown little change in the onset temperature of the endotherm or its height, as has been discussed in Ref. [129]. So, the endotherm observed in the DSC scan is unambiguously attributable to the glass-softening of ASW and HGW. A recent study seems to confirm it [93].

There has been a further development, which came from the use of DSC scans in the calorimetric study of ice XII. Salzmann et al. [130] found that both the unannealed ice XII and annealed ice XII recovered at ambient pressure show an endothermic feature in their DSC scans obtained by heating at 30 K min^{-1}. They concluded that this is "in line" with Handa et al. [126] observations by C_p measurements of the unannealed and annealed ices V and VI, and therefore Salzmann et al. [130] used it as a criterion to speculate that similar features observed for LDA [29,104] could have been possibly made on ice XII. However, their Fig. 4 in Ref. [130] shows that the DSC scan's peak height and probably also the area do not show a systematic change with increase in the annealing time. They also repeated Handa et al.'s [126] study for ice V by DSC and the scans for ice V in their Fig. 9 also show no systematic change of the peak height or area with the annealing time. This is contrary to the findings by Handa et al. [126] who had found clear and systematic changes in the peak height and area on annealing of ices V and VI [127]. To resolve this aspect further, it seems necessary to determine the relaxation time of LDA at ambient pressure by dielectric or NMR methods.

Since Salzmann et al's [130] conclusion has a bearing on the earlier studies of LDA [29,104,131], another more recent observation is worth mentioning here. In a paper on proton-ordering of HCl-doped ice V, Salzmann et al. [132] have concluded that proton-ordering in pure ice V "could not be confirmed by Raman spectroscopy" and "...similar endothermic events were also found for ice XII". This conclusion creates doubts regarding the source of the endothermic feature observed for ices V and XII. In our view, this restores the interpretation of the DSC feature for LDA [29,104,131].

There have also been attempts to observe molecular mobility in HDA and LDA by neutron scattering methods. Koza et al. [133] have performed a detailed and elegant study of HDA and LDA by measuring the intensity at $\omega = 0$ (see their Fig. 2). They have found that a pronounced drop-off in this intensity was not detected in the temperature range of crystallization of LDA to ice Ic at $T > 135$ K, where they had expected to find its T_g. On the basis that such a drop-off of intensity is a "fingerprint for an enhancement in molecular mobility of the sample", they deduced that its absence indicates that there is no molecular mobility in the LDA sample in the 135–155 K range at time scales of less than a few nano-seconds. Further studies of the energy scans obtained by the incoherent scattering technique confirmed that translation diffusion of molecules over intermolecular distances in LDA on a time scale of less than ∼4 ns does not occur during its transformation to ice Ic on heating through the 130–150 K range. They also found that LDA as well as ice Ic behave as harmonic solids.

The experiment time scale in the neutron scattering studies is of course longer than in the DSC studies of 30 K min^{-1}, which had showed its T_g to be first ∼129 K [29,104,131], and later ∼135 K [130]. Therefore, one expects that the enhancement of molecular mobility in LDA in the neutron scattering studies would be observed at a much lower temperature than 130 K. But the intensity at $\omega = 0$ in Fig. 2 of Ref. [133] also does not show a pronounced drop-off at lower temperatures. Since crystallization is usually a thermally activated process, the lack of any indication of molecular mobility in the temperature range of crystallization indicates that LDAs crystallization is a diffusionless process and thus unrelated to the viscosity of the material. In that case, the Johnson–Mehl–Avrami equation would not fit the crystallization kinetics data of LDA, and this aspect can be tested for LDA. There seem to be difficulties in resolving the issue of molecular translational diffusion in LDA and perhaps it may be worthwhile to determine if the harmonic solid behaviour of LDA found in these studies [133] is consistent with LDAs coefficient of thermal expansion in the 75–135 K temperature range.

In another aspect of the study, Johari [134] has argued that Fisher and Devlin's [135] findings of isotopic exchange can be explained by a mechanism in which H_2O clusters diffuse by first breaking hydrogen bonds from the neighbours, diffusing as whole and then reforming hydrogen bonds with other neighbours. It is also uncertain whether or not the presence of short-range order arising from hydrogen-bonded OH_4 tetrahedra

has an effect on the interpretation of scattering measurements in terms of molecular mobility [133]. This can be tested by studying SiO_2 and GeO_4 glasses which have a similar short-range order, but of SiO_4 and GeO_4 tetrahedra.

Studies have shown that a blunt indentor penetrates through 2–3 mm-thick sample of LDA on heating through the 142 K range [136], and therefore LDA deforms by viscous flow. In support of an alternative conclusion, it has been suggested that this finding is an effect described as "Indeed a tungsten wire can slice rather rapidly through crystalline ice samples, at temperatures several degrees below bulk melting point" [137]. We point out that a wire under a load traverses through ice Ih because dT_m/dP of ice Ih is negative. The ice refreezes after the wire has traversed through it, thus leaving the ice unsliced. This is not the case for LDA, which has no melting point, and it is well known that T_g of materials usually increases with increase in pressure. More experiments and/or interpretation are needed to resolve this issue. This is particularly important in view of the recent dielectric relaxation time measurements of LDA [110].

Finally, we consider a recent ultrafast microcalorimetry study of 1 ± 0.1 μm thick film of vapour-deposited, porous amorphous solid water (PASW) by calorimetric scans obtained by heating the film at a rate of $(1.3 \pm 0.2) \times 10^{5}$ K s^{-1} [137]. The study has concluded that most of the earlier findings on sintered amorphous solid water (ASW), hyperquenched glassy water (HGW) and low-density amorph (LDA) are inconsistent with the new data [137], and consistent with a disputed conjecture that the T_g of water is 165 K and cannot be measured. It was also reported that PASWs enthalpy relaxation time is greater than 10^{-5} s at 205 ± 5 K. We note that, in contrast to earlier studies in which 10–20 mg samples were used, experiments on PSAW in Ref. [137] were performed on ∼1–2 μm thick films and the consequent large surface effects in the porous samples are difficult to interpret. However, there are certain basic aspects of the study that have been overlooked. We briefly describe these here. In doing so, we, unlike in Ref. [137], do not use the terms ASW, HGW and LDA interchangeably. As discussed above, Hallbrucker et al. [26] had already shown the importance of sintering ASW prior to obtaining the DSC scans. In the Introduction section of that paper they reviewed the earlier studies in which the various time-dependent thermal effects observed on heating unsintered ASW or PASW were either confused with a prominent T_g-endotherm, or else taken for a lack of observation of a T_g-endotherm in the DSC scans. This paper may be consulted for details [26].

One aspect that has been overlooked in Ref. [137] is an unusually large increase in the temperature-width of the structural-unfreezing endotherm (not the T_g endotherm as reported in Ref. [137]) for toluene, which was used as a test liquid for ascertaining the merits of the ultrafast calorimetry technique. Briefly, the width of the endotherm, taken from its designated "T_g" and the peak position, for vapour-deposited porous toluene measured for heating at 1.3×10^{5} K s^{-1} rate in Fig. 3, Ref. [137] is ∼30 K. We point out that this width is 10 times the width of ∼3 K observed for bulk toluene [138] in the range of its structural-unfreezing at normal T_g of 117.5 K, as determined by heating at 10 K min^{-1}. One realizes that a decrease in the temperature sensitivity of the relaxation time with increase in temperature may make the endotherm somewhat broader for a higher heating rate as well as shift it to a higher temperature. But the distribution of relaxation times is also less at higher temperatures, which would make the width smaller. This is a well-known calorimetric effect and has been discussed in Ref. [139]. The 10-fold increase in the temperature-width of the T_g-endotherm for toluene is unusual and seems to indicate extrinsic effects associated with the ultrafast measurement technique used. To further elaborate, if we use this factor to scale the corresponding width of 14 K reported for the T_g endotherm for ASW [26], and ignore a possible decrease in the width due to decrease in the distribution of relaxation times, or assume the decrease to be about the same as for toluene, the expected width for PASW would be 140 K for heating at 1.3×10^{5} K s^{-1} rate.

We recall that C_p of ASW is within 2% of the C_p values for ices Ic and Ih up to a temperature of 125 K [99,140,141], and their C_p values are expected to remain close to each other as long as structural-unfreezing of ASW does not occur. The net increase in C_p for the 136 K T_g-endotherm is found to be only 8% higher than that of ice at its maximum value reached at 147 K [141], when ASW was heated at 30 K min^{-1}. It would be less if the sample was not fully amorphous. This is important because the PASW sample was stated to be at least 50% amorphous [137]. In that case, the sample would show a very broad T_g-endotherm, as explained above, with C_p rise of significantly less than 8% above the value for the ice. The noise in the data reported in Fig. 6 of Ref. [137] is comparable with that, and therefore it would obscure any slow increase of the wide C_p endotherm before the sample crystallizes.

The issue of the apparent absence of C_p-rise was considered in Ref. [137] in order to infer that the expected C_p-rise is enough to be observable. But in that consideration, interpolated paths of conjectured C_p in its plots against T in the supercooled region of water given in Ref. [142] were used. The three $C_p - T$ paths conjectured there had been originally used for analysing the continuity of states between HGW and ambient water [142] and they are valid only if the C_p of HGW is 2 J mol^{-1} K^{-1} higher than that of ice Ih at 153 K, as shown in Fig. 4 of Ref. [142]. If it is less than that, as Chonde et al.'s data [137] apparently suggest, then the paths in that Fig. 4 are inappropriate for resolving this issue. Moreover, as the ultrafast microcalorimetry technique broadened the structural-unfreezing endotherm for the test liquid, toluene, it would also broaden the corresponding endotherm for PASW and thus further reduce the C_p-rise of PASW before it crystallizes. It has also been stated that [137], "...the ASW content in our vapour-deposited ice films is at least 50%, which is sufficiently high to observe endothermic heat capacity variation". The amount of PASW in the sample is not known, but even if it is taken to be 70%, the reduced fraction of PASW and the exceptional broadening of the T_g-endotherm would make the endothermic signal smaller and hence even more difficult to discern by ultrafast technique used. Above all, we find that the data for the relaxation time of toluene used for testing the method's validity were compared by mistakenly using at least 100-times higher values than those in the literature they had cited.

Recent studies of the dielectric relaxation time of ASW and HGW have made it clear that their T_g is less than 140 K [118,119]. There is no experimental evidence to support the conjecture that ASWs T_g is ∼165 K. Since Hallbrucker et al. [26] had found it necessary to sinter the ASW sample prior to studying its DSC scans in order to reveal the T_g-endotherm, it may also be necessary to perform accurate measurements on sintered ASW samples using ultrafast microcalorimetry.

5. Characteristic changes during pressure-amorphization of ice

It has been known since the 1960s that a variety of materials can be converted from their crystalline solids to an amorphous state isothermally by uniaxial compression and most of those may be retained in the apparently amorphous state at very low temperatures at ambient pressure. The pressure-induced collapse of crystals may result from natural or man-made impact, from a shock wave generated by it, or from a sustained stress as in geological occurrences. Historically, as early as 1963, Skinner and Fahey [143] had reported that stishovite, a form of crystalline silica, becomes amorphous by the simple procedure of mechanical grinding, and others had reported similar observations for other crystals soon thereafter [144]. In his compilation of the properties of silica, Primak [145] had noted that under a shock pressure of more than 20 GPa, SiO_2 becomes amorphous. In 1972, Brixner [146] reported that $Gd_2(M_2O_4)$ crystals become amorphous when subjected to pressure. Since 1981, there have been a number of systematic studies of shear-induced mechanical amorphization of metal crystals in a high-speed ball mill, in which crystals were subjected to high impact [147,148]. Hemley et al. [149] reported that α-quartz and coesite crystals at 300 K transform to amorphous solids at 25–35 GPa and 300 K, indicating the thermoelastic instability of tetrahedral network structures at high compression. Their amorphous structure has been generally deduced from the observation that their X-ray and neutron diffraction features lack sharp features or Bragg peaks, or their vibrational features show exceptional broadening of the peaks. A brief description with relevant references to earlier studies of pressure-amorphization of a host of materials is given in the Introduction of a recent article [150].

During the course of the collapse of a crystal, topological arrangement of atoms or molecules is forcibly altered by the applied pressure, which in the case of ices Ih and Ic would correspond to a value greater than the value of their Young's moduli. But, more significantly, while the density decreases on amorphization of a crystal, the density increases on pressure collapse and subsequent amorphization, while the internal energy increases in both cases. When the resulting change in the molecular arrangement leads to random displacement of molecules in the structure, the collapsed solid may appear amorphous in the X-ray and neutron diffraction spectra. But when it leads to formation of nanometer size crystals of high-pressure phases of ice, with a very large net surface area, the product formed after the collapse has a higher density and would still appear amorphous in the X-rays and neutron diffraction spectra. In this context, it should be noted that recent studies of HDA and LDA have shown a considerable scattering of neutrons at small angles, i.e., at low q values [36] that has been attributed to the heterogeneous disordered structures of HDA at a mesoscopic scale. This is similar to a feature that had been observed earlier in the neutron scattering studies at small angles when water was confined to the nanopores of a polymer [151]. Koza et al. [36], have linked this low angle scattering feature to the diversity, heterogeneity and kinetics of the HDAs and LDA, and have suggested that there may be only one HDA. The latter is consistent with an earlier conclusion [34,152] that there are only two solid amorphs, one is known as LDA and the other is known as "very high-density amorph" (VHDA), both are seen as mesoscopically homogeneous phases. Other HDAs of intermediate densities are therefore mesoscopically heterogeneous structures. Density of VHDA has been measured at ambient pressure and 77 K by recovering a sample that had formed when HDA at 1.1 GPa had been heated to 165 K [74]. It has also been determined by using the piston displacement data during pressurizing of LDA at 125 K to 1.5 GPa [153,154]. In both cases, it seems doubtful that the ultimate density had been reached. It is known that the volume does not change at glass–liquid transition, and therefore the density of the ultimately formed VHDA would be close to that of the ultraviscous water at 140 K and ∼1 GPa, but this density is not known, even though its dielectric relaxation time is known [53,54]. Although the density of VHDA has been determined by the buoyancy method at ambient pressure and also piston displacement measurements at high pressures have been reported, these values have been revised and more recent data indicate that VHDA produced on pressurizing LDA at 125 K does not reach the limiting high-density value [153,154]. Whichever state of HDA has been formed by pressure collapse of ices Ih and Ic, most studies have shown that properties of this state change irreversibly with pressure and temperature.

In this context we recall that HDA was accidentally discovered when ice Ih contained in a piston cylinder apparatus at 77 K [27,28] was found to irreversibly collapse on raising the uniaxial pressure on it to ∼1.5 GPa. The experiments were similar to those performed on ice clathrates a few years earlier by Ross et al. [71]. Since tetrahedral hydrogen bonding in the open structures of ices Ih and Ic is much weaker than the covalent bonding in SiO_2, the structure of these ices at 77 K collapses at a relatively low-pressure of ∼1 GPa with a density increase from 0.93 to 1.31 g cm^{-3} at 77 K and 1 GPa [27,28]. It was earlier thought that at 77 K, ice Ih slowly melted irreversibly at ∼1 GPa pressure, and the slow crystal–liquid transformation was thermodynamic in nature. If so, it was expected that tetrahydrofuran ice clathrate would show a similar transformation at a much lower pressure of 0.3–0.4 GPa of its extrapolated phase boundary [56]. But studies of volume and dielectric properties of tetrahydrofuran ice clathrate showed no indication of its pressure collapse. A further study showed that it was not possible to recover the high-density phase of the ice clathrate at zero pressure, as it reverted to the original crystalline structures when the pressure was released [155]. It is still unclear why a high-density amorph cannot be obtained from pressure collapse of an ice clathrate,

whose structure is as bulky as that of ices Ih and Ic, and, if a high-density amorph does form, why it cannot be recovered at ambient pressure at 77 K.

It is to be noted that when the pressure on the collapsed state (of unknown structural details, homogenous or inhomogeneous, highly deformed or nano-crystalline mixture of various ices, mixture of the ices with non-crystalline solid, or even mostly non-crystalline solid, showing no Bragg reflections) is decreased, the sample does not transform back to ice Ih and the state recovered at ambient pressure remains amorphous. A noteworthy parallel to this occurrence is mechanical deformation of crystals in a high-speed ball mill, which also amorphizes a crystal if vitrification temperature of the amorph is much lower than the ball-milling temperature. In either case, the collapse of ices Ih and Ic, occurring at low temperatures when the product is a rigid solid, produces a structure of fixed configuration, like that of a nonergodic state. Therefore, only the vibrational or non-relaxational properties of the sample change as a result of changing structure of the sample during its collapse. Also, as long as the temperature of the collapsed state is kept low, the change in its properties on cooling and heating is vibrational in origin, occurring reversibly, as the structure does not change. X-ray and neutron diffraction features of the HDA samples recovered at ambient pressure at 77 K have shown differences in the details of the structure factor studied by the same group as well as by different groups, as was discussed earlier [34]. It was concluded that lack of control of pressure, temperature and time conditions has led to such differences, and that there is no single HDA that is produced by pressure collapse of ice Ih [34]. Ice Ic has also been found to collapse under pressure to produce HDA, but the pressure is slightly less than that for collapse of ice Ih [31].

In addition to measuring the volume from piston displacement data, progress of the collapse of ice Ih has been investigated by measuring the thermal conductivity, the ultrasonic sound velocity and the limiting high-frequency permittivity, a measure of the infrared-red polarization. The plots for the piston displacement in a pressure vessel containing ice Ih at 77 K are shown in Fig. 8(A), of the limiting high-frequency permittivity at 77 K in Fig. 8(B), of the thermal conductivity at 130 K in Fig. 8(C) and of the velocity of transverse sound waves of 5 MHz frequency at 77 K in Fig. 8(D).

To determine if the pressure collapse of ice is influenced by the crystal size, experiments have been performed by freezing water, which produced up to 0.5 mm size crystals, by transforming ice Ic to microcrystalline ice Ih, and by allowing the micron-size crystals of ice Ih formed from ice Ic to grow to a relatively large size. These experiments have revealed that millimeter-size crystals begin to collapse at ∼1 GPa at 77 K and micrometer-size crystals at ∼0.7 GPa. This shows that the pressure needed to collapse the structure of ice Ih decreases as the crystal size is decreased or as the ratio of surface to bulk energy is increased. Johari has reported [31] that in his crude attempt, a nominally 2 mm diameter, 3 mm long single crystal of ice Ih at 77 K did not collapse at ∼2 GPa pressure, thereby suggesting that polycrystallinity of a sample has a role in its pressure collapse.

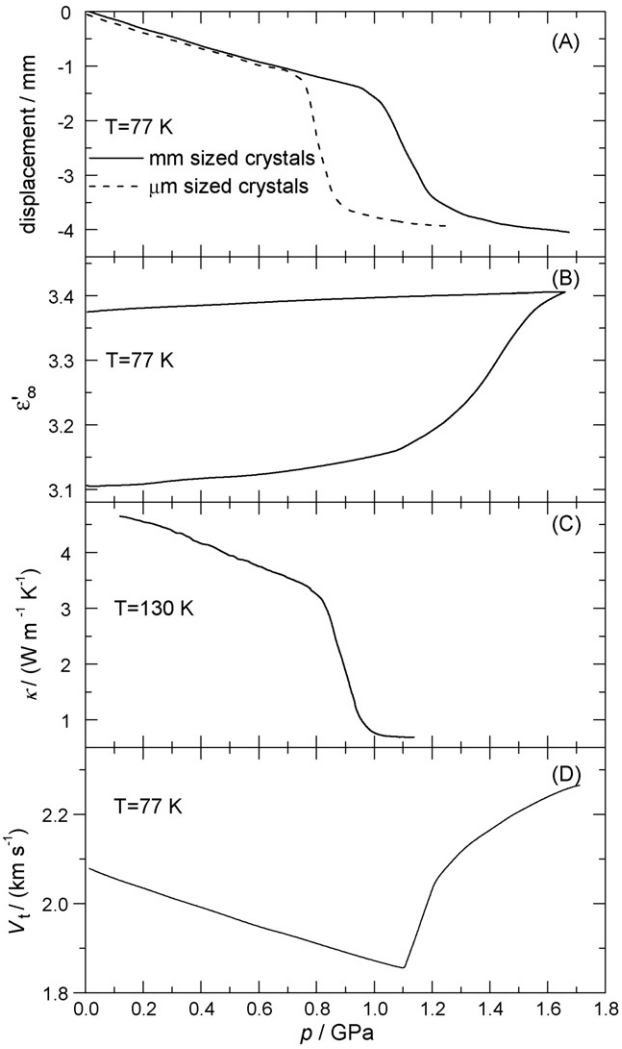

Fig. 8. Changes in the properties of ice Ih on increase in the pressure showing the effect of collapse or amorphization of ice under a uniaxial pressure that is expected to become hydrostatic by mechanical deformation of ice. (A) Volume decrease indicated as displacement of the piston in the pressure vessel containing ice Ih crystals of millimeter size and micrometer size at 77 K. Data are taken from Ref. [31]. (B) Increase in the limiting high-frequency permittivity at 77 K. Data are taken from Ref. [56]. (C) Decrease in the thermal conductivity of ice Ih at 130 K. Data are taken from Ref. [152]. (D) The increase in the velocity of transverse sound wave at 77 K. Data are taken from Ref. [32]. Note that increase in pressure irreversibly transforms crystalline ice to an amorphous structure, i.e., it does not transform back to the crystal phase on removal of pressure. Nevertheless, the transformation is cyclic in that the amorphous solid can be heated to obtain the original crystal phase which then can be cooled and pressure-amorphized again.

During the pressure collapse of ice Ih, the limiting high-frequency dielectric permittivity, ε'_∞ which contains no relaxational contribution, has been found to increase gradually in a sigmoid-shape manner from 3.1 to 3.4, as seen in Fig. 8(B). Decompression of the sample does not restore the original value, and ε'_∞ of the pressure-amorphized solid remains at about 3.36 [56]. This increase from 3.14 to 3.40 on pressure collapse is partly due to the increase in the square of the optical refractive index from 1.73 to 1.79, as the density increases from 0.93 to 1.17 g cm^{-3}, but it is mainly due to the increase in the infrared

(vibrational) contribution to ε'_∞, i.e., the frequency of translational vibrations in the pressure collapsed solid is lower than in ice Ih and/or the absorptivity associated with these vibrations is higher. This observation led to the inference [56] that the near neighbour distance between the water molecules in HDA should be greater than in ice Ih, which was confirmed from determination of the near neighbour distance from X-ray diffraction of the pressure-amorphized solid by Bosio et al. [156], but there have been no studies of the infrared spectra during the pressure collapse of ice Ih to confirm the inferred lowering of this vibrational frequency.

Yoshimura and Kanno [157] have performed an *in situ* study of the Raman spectra of ice Ih during the course of its pressure-amorphization. They found that the 3082 cm^{-1} peak which is the most prominent peak of ice Ih at ambient pressure and 77 K decreases in height and shifts to lower frequencies as the pressure is increased slowly to 0.9 GPa, and then vanishes at 1.2 GPa, while the 3200 cm^{-1} small peak broadens and become most prominent at 1.2 GPa. Yoshimura and Kanno [157] attributed this finding to formation of strong hydrogen bonds in HDA. They further concluded that amorphization of ice Ih to HDA is not a transition to a glassy state of high-density water at 1.2 GPa, but is a process of collapse of the structure at high pressures. Heating of HDA at 1.2 GPa to 218 K produced ice VI (ice IV written in their paper is probably a transcription error) and heating HDA at 1.2 GPa to 153 K and also at 0.7 GPa to 153 K made the broad peak and the high-frequency shoulder more prominent, with a slight shift of both features to a higher frequency, indicating densification of HDA. These observations were reflected in a dilatometric study [74], which led to the naming of densified sample as VHDA.

There is, however, an interesting feature in Fig. 2 of Yoshimura and Kanno [157], which is worth noting. During the shifting of the ice Ih 3082 cm^{-1} peak to lower frequencies on increase in pressure at 77 K, the shift is highest when p is increased from 170 to 260 MPa. It is also much greater than the total shift on raising p from 260 to 900 MPa, suggesting that something other than simple compression occurs in the 170–260 MPa range. But if the pressurization rate was not constant and more time elapsed in raising p from 170 to 260 MPa than at other pressures, the additional change in the sample's state would be due to the longer time taken in the 170–260 MPa range. Significance of this observation would perhaps be made clearer in future experiments using the same or another technique.

Andersson and coworkers [34,50] have studied the progress of pressure collapse of ices Ih and Ic by measuring the thermal conductivity in real time, and Brazhkin and coworkers [158–160] have studied the velocity and attenuation of ultrasound waves. Thermal conductivity, κ, of both ices Ih and Ic has been found to decrease on increase in the pressure according to broad inverted sigmoid shape plot, as shown in Fig. 8(C), in remarkable similarity to the shape of the piston displacement or the volume against pressure plot for the ices shown in Fig. 8(A). The plot of κ against pressure at 130 K in Fig. 8(C) shows about the same onset pressure of ∼0.8 GPa for the collapse of the structure as the plot of the piston displacement of micron-size crystals of ice Ih. This indicates that the effect of increase in the temperature on the onset pressure for collapse is similar to the effect of decrease in the crystal size, or increase in the net surface (interfacial or grain-boundary) energy of the ice sample. This is a remarkable finding in that it suggests that thermal energy has a role qualitatively similar to the surface energy. We conclude that in terms of the high pressure needed, it is easier to collapse ice Ih by either decreasing the crystal size or increasing the temperature of the sample.

Gromnitskaya et al. [32] have reviewed in detail the studies of the velocity of sound waves performed by their group. They showed that the velocity of sound waves and shear modulus increase sharply as the ice Ih structure at 77 K collapses under pressure, and the bulk modulus increases [32]. The plot of the (transverse) ultrasonic velocity against pressure constructed from Gromnitskaya et al.'s data [32] in Fig. 8(D) shows that the ultrasonic velocity increase is abrupt, and much sharper than the changes observed in the volume, thermal conductivity and limiting high-frequency permittivity, as seen in Fig. 8(A)–(C). This indicates that the pressure collapse of ice Ih in their experiments is initially very sharp. This is quite the opposite of the spread-out pressure range for the collapse indicated by the broad-shape plots observed in the volume, thermal conductivity and the high-frequency permittivity measurements. The reason for such a sharp change has remained unclear.

Crystals of ice Ih are mechanically anisotropic. They deform more easily along the basal plane than along a plane normal to it [113] and thus it seemed plausible that, owing to this anisotropy, pressure causes stress concentration at some grain junctions, and thus collapses its polycrystalline sample. But experiments performed on mechanically isotropic crystals of ice Ic [29,30] have shown that its polycrystalline sample at 77 K and at higher temperatures [50] also collapses under pressure. Fig. 9(A) shows the plots of κ against pressure for ice Ih at 115 K and 129 K and for ice Ic at 129 K. An LDA sample was also made by depressurizing HDA at ∼130 K to a pressure below 0.05 GPa. Its κ at 129 K is also plotted in Fig. 9(A). Here, the sigmoid-shape decrease in κ on pressure collapse of the two ices and LDA is clearly evident, but the plots also show that this shape becomes narrower when the temperature of ice Ih is raised from 115 to 129 K and the onset pressure for the collapse decreases from 0.9 GPa at 115 K to 0.8 GPa at 129 K. (Note that a further effect appears here as a jog at a pressure of ∼0.9 GPa for the 115 K plot. This jog from the smooth, sigmoid-shape curve was caused by the inadvertent waiting at this pressure for an unknown period. Its occurrence is significant, as it indicates that pressure collapse continues isothermally at a fixed pressure, and it has led us to study the time-dependence of the pressure collapse of ice Ih, which would be described later here.) The onset pressure for collapse of ice Ic at 129 K is ∼0.1 GPa less than that for ice Ih, the grain size in both cases remaining large. Thus loss of mechanical anisotropy in going from ice Ih crystals to ice Ic crystals serves to lower the collapse-pressure of their structures, not increase it. This is also borne out by the finding that the disordered bulkier structure of LDA, which is mechanically isotropic, collapses at a much lower pressure of ∼0.35 GPa at 129 K, as is seen as the small sigmoid shape decrease in κ in Fig. 9(A). The decrease in

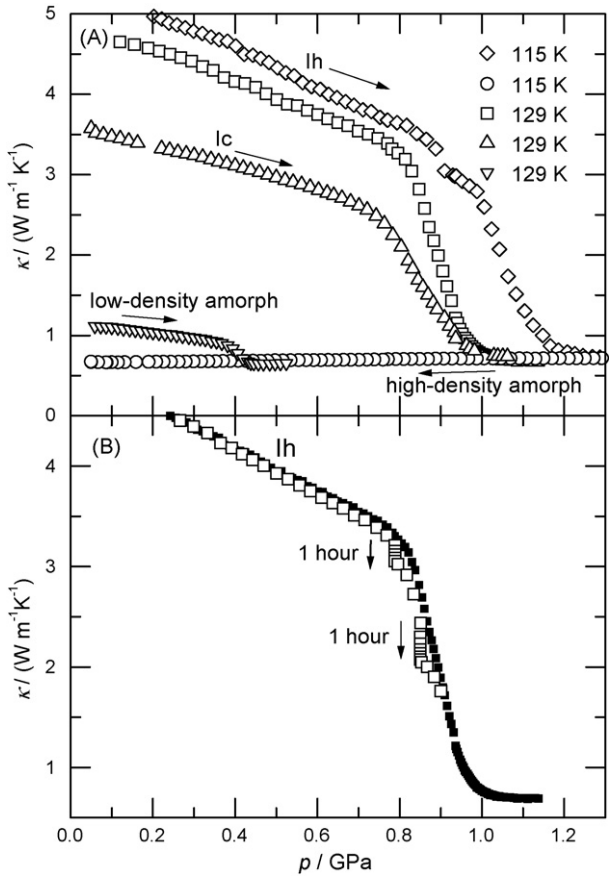

Fig. 9. (A) Thermal conductivity of ice Ih at 115 and 129 K and of ice Ic at 129 K is plotted against the pressure showing their respective collapse or amorphization ranges, and the thermal conductivity of the pressure-amorphized solid on lowering the pressure to ambient. The jog from the smooth sigmoid shape in the plot for 115 K near 0.9 GPa is caused by the inadvertent waiting at this pressure for an unknown period. The plots show that the onset pressure for amorphization decreases with increase in the temperature and is about 0.1 GPa lower for ice Ic at 129 K than for ice Ih. Data are taken from Refs. [50,152]. (B) Thermal conductivity of ice Ih at ∼130 K is plotted against the pressure. The vertical arrows during the course of amoprhization are for fixed pressure conditions of 0.8 and 0.85 GPa at which the sample was kept for 1 h after the pressure-amorphization had begun. Data are taken from Ref. [34].

the collapse onset pressure on increase in temperature of ice Ih is particularly significant, as it means that this pressure decreases when thermal energy of ice Ih is increased. This is the opposite of the effect observed for vitrification of liquids, because the pressure required to vitrify a liquid increases as the temperature is increased. The plot in Fig. 9(A) shows that κ of the pressure collapsed solid decreases when the pressure is decreased, an aspect discussed here in connection with the results in Fig. 3.

6. Time-, pressure- and temperature-dependence of the extent of amorphization

The plot of κ against the pressure in Fig. 9(B) shows the stepwise manner in which ice Ih collapses, when the pressure is raised incrementally. In this experiment, κ of an ice Ih sample at 130 K was first measured as its pressure was slowly raised to 0.8 GPa, which is a higher pressure than the onset pressure for the collapse leading to amorphization, and then measured with time for 1 h as the sample was kept at 0.8 GPa. The decrease in κ is shown by an arrow. The sample's pressure was raised to 0.85 GPa and the measurements made for another 1 h. The decrease observed is also shown by an arrow. Finally the pressure was slowly raised to completely amorphize the ice. For comparison, another sample of ice Ih was studied by continuously increasing the pressure at the same rate and its results are shown by filled squares in Fig. 9(B). The study shows that once ice Ih has been brought to a pressure in the (collapse) amorphization range and kept at that pressure isothermally, the amorphization process becomes time-dependent at a fixed T and p and that the amount amorphized in 1 h, as indicated by the vertical decrease in κ, is more at 0.85 GPa than at 0.8 GPa.

This time dependence is an important aspect of the pressure-amorphization mechanism, particularly as it contradicts the currently held presumption that ice Ih to HDA is a thermodynamic transformation with an equilibrium pressure of 0.5 GPa at 77 K for the purpose of constructing the equilibrium phase diagram [44,161]. Merit of this phase diagram was questioned in Ref. [83] where it was shown that HGW and LDA are two solids with different thermodynamic properties. Since HDA is not the equilibrium state, but only one of the intermediate states, transformation between ice Ih and HDA is not an equilibrium transition at 0.5 GPa and 77 K. It also shows that the state formed depends on the thermal and compression histories of the sample. Because of its significance, the time-dependence of this process has been studied in detail by continuously measuring κ of ice Ih in real time at a fixed temperature and fixed pressure over a period of several days. In a typical experiment, ice Ih was kept at 128 K and 0.8 GPa and its κ was measured over a period of 110 ks (30.6 h). Its value is plotted against time in Fig. 10(A). It shows a much larger decrease in κ over time and the decrease itself occurs in an asymptotic manner, but with little indication of an approach to a limiting low value in an experimentally convenient time. Further experiments were performed on ice Ih for other p–T conditions and for different time periods. The data obtained for six such conditions are shown in Fig. 10(B) and (C).

In general, the time-dependence of a property during the pressure collapse indicates one or several of the four following occurrences: (i) crystallites in the polycrystalline sample collapse at different rates by a mechanism that continuously changes the conditions required for their collapse with time, (ii) the sample becomes a mixture of crystallites and their collapsed state at its initial stages, (iii) all the crystalline sample has collapsed but the state formed is kinetically unstable and is tending toward a more stable state at high pressures, and (iv) highly deformed crystallites or else a mixture of nanometer-size crystals of high pressure polymorphs of the material have formed whose deformation or composition continuously changes with time. In occurrences (i) and (ii), the rate of approach to a stable state is expected to be very small in the early period immediately after the onset of collapse because the amount of the collapsed state formed would be negligibly small. It would become significant only when most of the sample is in the collapsed state. In their physical manifestation, occurrences (iii) and (iv) are analo-

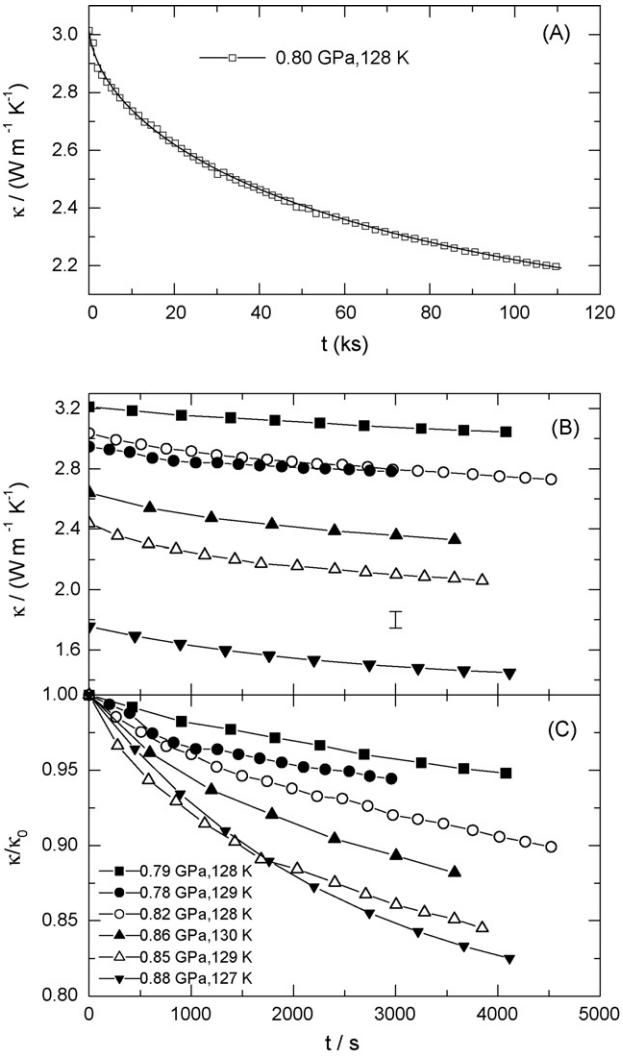

Fig. 10. (A). Thermal conductivity of partially collapsed or amorphized state of ice Ih at 0.8 GPa and 128 K. The line is calculated from stretched exponential relation given here. Data are taken from Ref. [73]. (B) Thermal conductivity of several samples plotted against time. Data are taken from Ref. [73]. (C) Normalized values of the measured thermal conductivity with respect to the initial (zero time) value of the samples kept at different pressures and temperatures are plotted against time. The pressure and temperature conditions are as labelled. Data are taken from Ref. [152].

gous to structural relaxation of the state obtained by mechanical amorphization of crystals in the high speed ball-milling process, to structural relaxation of a glass formed by hyperquenching the melt, or to structural relaxation of an amorphous solid made by vapour-deposition. All the three states have high energy and high fictive temperatures. They become denser spontaneously with time, as their amorphous states approach asymptotically an amorphous structure of lower energy and lower fictive temperature. In the plots in Fig. 10(B), κ at various conditions of fixed p and fixed T is also seen to decrease asymptotically with time towards a limiting low value. It is clearly evident that κ of the sample as well as the rate of the asymptotic decrease in κ with time varies with the p–T conditions.

To help discuss specifically the pressure collapse and amorphization of ice Ih, each set of measurements given in Fig. 10(B) is converted to the normalized value $[\kappa(t)/\kappa(0)]_{p,T}$, and is plotted against the time, t, in Fig. 10(C). It is evident that $[\kappa(t)/\kappa(0)]_{p,T}$ decreases with time, and tends toward $[\kappa(\infty)/\kappa(0)]_{p,T}$, that is different for different p–T conditions. The plots in Fig. 10(C) also indicate that $[\kappa(t)/\kappa(0)]_{p,T}$ values at a given time differ even when the p–T conditions are almost the same, as for the plots at 0.86 GPa and 130 K and 0.85 GPa and 129 K. This finding means that the collapse-rate, which probably but not necessarily reflects amorphization rate, differs even when p–T conditions are closely similar. (As increase in density increases κ of HDA [50], a process involving only relaxation of HDA to a higher density would be inconsistent with the observed decrease in κ with time.) Moreover, the plot for 0.85 GPa and 129 K and that for 0.88 GPa and 127 K cross over, thus showing that there is a time reached at which $[\kappa(t)/\kappa(0)]_{p,T}$ is the same for different p–T conditions, although the rate of decrease in $[\kappa(t)/\kappa(0)]_{p,T}$ with time differs. Clearly, a given value of κ of the sample can be reached by different p–T–t paths. Altogether, these findings indicate that the initial p, T conditions determine the rate of ice Ih structure's pressure collapse and that the amount of the collapsed state or the extent of amorphization at a given p, T and t, as indicated by the κ value, is determined by more variables than have so far been considered in such studies.

The asymptotic nature of the decrease in thermal conductivity with time at 0.8 GPa and 128 K seen in Fig. 10(A) can be described by a stretched exponential relation,

$$\kappa(t) = \kappa(\infty) + [\kappa(0) - \kappa(\infty)] \exp\left[-\left(\frac{t}{\tau_{0,\kappa}}\right)^{\beta}\right] \quad (7)$$

where $\kappa(0)$ is the value of κ at the instant when the fixed pressure experiment at 0.8 GPa was begun, $\kappa(\infty)$ the limiting long time value of κ, and $\tau_{0,\kappa}$, the characteristic pressure collapse or amorphization time. The fit of Eq. (7) to the data is shown by the smooth line in Fig. 10(A). The normalized value of the same data is plotted against logarithmic time in Fig. 10(C). The values obtained from this fit are $\kappa(0) = 3\,\mathrm{W\,m^{-1}\,K^{-1}}$, $\kappa(\infty) = 1.8\,\mathrm{W\,m^{-1}\,K^{-1}}$, $\tau_{0,\kappa} = 90.9$ ks (1500 min) and $\beta = 0.6$. From these parameters we calculate that, at 0.8 GPa and 128 K, it would take 120 h to reach a state whose κ value is within 5% of the $\kappa(\infty)$ value of $1.8\,\mathrm{W\,m^{-1}\,K^{-1}}$. Moreover, the plots in Fig. 10(C) show that at 0.8 GPa and 128 K, κ of the state formed would not decrease to the same value as that of the state formed at 1.15 GPa and 129 K in the plot of Fig. 9(A). To elaborate, κ of the state formed at 1.15 GPa and 129 K is $\sim 0.7\,\mathrm{W\,m^{-1}\,K^{-1}}$ in Fig. 9(A), but $\kappa(\infty)$ of the state formed at 0.8 GPa and 128 K is $1.8\,\mathrm{W\,m^{-1}\,K^{-1}}$, i.e., $1.1\,\mathrm{W\,m^{-1}\,K^{-1}}$ higher. Therefore, it would seem that either the collapsed state of ice Ih or the HDA formed after keeping for a formally infinite time at 0.8 GPa and 128 K would be different from that formed at 1.15 GPa and 129 K, or Eq. (7) does not apply for the entire transformation. In this context two findings are significant: (i) κ of the state formed by slow pressurization to 1 GPa at 129 K [34] increases only slightly on heating, which is due to an inherent increase of HDA's κ with T and not due to a concurrent increase in the density on HDAs conversion to VHDA [74], because VHDA was formed already during slow pressurization at high temper-

atures in our experiments, and (ii) the denser state recovered at ambient pressure has different X-ray diffraction features (see Ref. [152] for discussion). Based on these findings, we conclude that the final state attained on pressurizing ice Ih depends upon the p–T conditions. If the sample is kept at 0.8 GPa and ∼130 K even for an almost infinite time, the final state would likely be inhomogeneous. However, the extent of inhomogeneity would decrease with annealing time and with increase in pressure, and the state formed after long-time annealing at 1.15 GPa and 130 K is likely to be homogeneous and close, or identical, to that recently referred to as VHDA [74].

As part of further analysis, α, the extent of conversion of ice Ih to the collapsed state has been calculated by using the thermal conductivity data measured with time in the relation,

$$\alpha(t) = \left(\frac{\kappa(0) - \kappa(t)}{\kappa(0) - \kappa(\infty)}\right)_{p,T} \quad (8)$$

and the plot of α against time has been found to have an extended sigmoid shape, resembling the shape of the extent of crystallization, phase transformation, chemical reactions and structural relaxation against time plots. This feature has been discussed in detail earlier [152].

It should be noted that equations similar to Eq. (7) have been fitted generally to the relaxation spectra in studies of molecular relaxation processes, to the enthalpy and volume changes in structural relaxation studies, and to the extent of transformation in chemical reaction kinetics. In all these studies, the quantity β has been found to be less than 1 and interpreted in terms of a broad distribution of relaxation times [162–164]. The distribution has been suggested to be due to microscopic dynamic heterogeneity in ultraviscous liquids and glasses [165–167]. In chemical reaction kinetics, it has been interpreted in terms of a diffusion-controlled kinetics, dispersive kinetics, or a distribution of the reaction rate constants. This latter idea was developed by Plonka [168], who has developed the concepts of dispersive kinetics of such (transformation) reactions [168], in which homogenization at a molecular level (in viscous liquids and glasses) does not occur over the time scale of the transformation. Consequently, a molecular level heterogeneity of the reactants and products develops within the bulk of a sample on the transformation time scale. An extension of Plonka's theory [168] to the amorphization process of ice Ih would mean that molecular level regions of the amorph and ice Ih exist in the bulk of the sample over the transformation time scale.

Raman spectra of ice Ih at 135 K and 0.7 GPa have shown features attributable to the presence of both ice Ih and HDA [169]. As expected, the OH-stretching peak of ice Ih shifts to a lower frequency [170]. The spectral sampling time and other parameters for measurements are usually kept the same in order to allow direct comparison of the spectra, and if that is the case then it is worth pointing out that the OH stretching peak intensity of ice Ih relative to that of pure HDAs broad peak at 1.2 GPa in Fig. 2, Ref. [169] indicates that at least 50% ice Ih remains with HDA at 135 K and yet the intensity for pure HDAs peak at 1.2 GPa is surprisingly not much more than that of the sample at 0.7 GPa. On pressurizing from 1.2 to 3.5 GPa, pure HDA at 135 K transforms to ice VII, and on depressurizing on ice VII at 135 K, the sample converts to LDA without forming HDA [169]. Since real time studies of the Raman and far infra-red spectra of ice Ih isothermally at a fixed pressure or with slowly increasing pressure are not available, we can only qualitatively discuss the types of changes occurring at various times during the pressure collapse or amorphization of ice Ih at a sustained high pressure. During this occurrence at, for example, 0.8 GPa and 129 K, the solid, as already noted in general terms above, may be, (i) a mixture of ice Ih and a certain unknown amount of the collapsed state or amorph whose $\kappa(\infty)$ is ∼1.8 W m^{-1} K^{-1}, (ii) a mixture of ice Ih and a certain unknown amount of a collapsed state or amorph whose $\kappa(\infty)$ is ∼0.7 W m^{-1} K^{-1}, (iii) entirely a collapsed state or an amorph that gradually transforms to its own $\kappa(\infty)$ value of ∼1.8 W m^{-1} K^{-1} at 0.8 GPa and 129 K, or (iv) a mixture of highly deformed ice Ih crystals, or else a mixture of nanometer-size crystals of high-pressure ices whose deformation and/or composition continuously changes with time. Of these, occurrence (iii) and (iv) may have produced "HDAs" with different X-ray and neutron diffraction and other features, as discussed earlier [34], and which would have led to a further increase in density to a state named VHDA, when an HDA state already formed by pressure collapse of ice Ih at 77 K and 1.45 GPa was isobarically heated at ∼1 GPa to 160 K [74].

To determine the relative merits of these possibilities, we recall that Hemley et al. [171] had reported changes occurring in the texture of the ice Ih at 77 K, as the pressure was increased in their diamond anvil high-pressure cell containing ice Ih. In particular, they observed extensive fracturing of the sample at ∼0.5 GPa and development of turbidity by the time the pressure had reached ∼1 GPa, and a new phase appearing along the fracture faults [171]. This indicates that ice Ih exists initially with a texturally different, turbid solid at least up to a pressure of ∼1 GPa. Salzmann et al. [130] have reported that X-ray diffraction spectra of the recovered sample at ambient pressure and 77 K contained distinctive features of both the amorphous solid and ice Ih, which means that their sample was a mixture of the amorph and ice Ih, as in (i) and (ii) above, and ignoring the possibility that some of the ice could have also formed during the handling of the samples.

The above-given occurrence (iii) requires that all ice Ih sample collapse or amorphize abruptly. But no study has shown that complete collapse or amorphization of ice Ih occurs abruptly and it seems inconceivable that near the onset of this occurrence, ice Ih and the collapsed state or the amorph would have the same thermal conductivity, thereby preventing us from detecting any abruptly occurring changes. It should also be noted that in one dilatometric study of 1–1.5 mm thick an ice Ih sample at 77 K, amorphization apparently occurred [172] first slowly and then abruptly, reaching completion at ∼1.06 GPa [172]. But we now know that when ice Ih is kept at a fixed pressure, that is far above the onset pressure, for a short period, the plot of the piston displacement against pressure in the collapse or amorphization range of both ices Ih and Ic would be vertical. This vertical plot can be mistaken as an indication of a relatively abrupt decrease in the volume. (Note that the jog in the plot of κ at 115 K in Fig. 9(A), or the vertical decrease in κ in Fig. 9(B) here could

have been mistaken as an indication of abrupt amorphization.) Since the rate of pressurization in the earlier study [172] had not been controlled, and an unknown period of time was allowed between pressure-increase steps, and further that this could lead to a feature similar to the one seen in Fig. 9. Therefore, we do not consider (iii) above as a probable occurrence.

Hemley et al.'s [171] real-time optical observations that, (a) ice Ih at 77 K, fractured under a hydrostatic pressure of 0.5 GPa, and (b) that it became turbid with further increase in pressure, are mechanistically significant because fracture of ice Ih at 0.5 GPa pressure would occur only if it transforms to a denser phase in preferred regions, and turbidity would develop if either crystals of different refractive indices are formed, or the size of ice Ih, high-pressure ices and amorphous regions are all small enough to scatter light. In either case, ice Ih crystals may coexist with the high-density ices or an amorph as in (i) or (ii) above. It is probable that ice Ih crystallites begin to deform and/or to recrystallize to nanometer size crystals of high-pressure ices at a certain pressure as mentioned in (iv) above, and the state formed shows no Bragg peaks. This occurrence is followed by the relaxation of the structure with time to a collapsed, or amorphous state at 0.8 GPa and 129 K. We conclude that structural relaxation at a fixed pressure may occur *via* a series of sequentially denser states of lower κ, until the final state of a characteristic κ value has been reached. One expects that the plots of piston displacement and of κ against pressure would not be identical because the process by which the mixture of nanometer size crystals of high pressure phases of ice forms would not be identical in different experiments performed at the same temperature and the same pressurization rate. Experiments have shown that such plots obtained in different experiments are not identical.

The fact that pressure collapse or amorphization of ice Ih is not thermodynamic in nature is also evident from a basic analysis of the properties of an equilibrium state. Briefly, when a material is in a thermodynamic equilibrium state, its vibrational and other properties are a state function, i.e., they are not determined by the path used to produce that equilibrium state. Therefore one would expect that the measured values of the density, ρ, as well as ultrasonic velocity, v_{trans}, of the HDAs obtained by pressure-amorphization of ice Ih would be the same irrespective of the temperature–pressure path used to obtain HDA, as discussed in Ref. [37]. Briefly, the analysis has shown that at 1.6 GPa and 77 K, the ρ values of the HDAs formed by different paths are spread over a 0.05 g cm^{-3} range, from 1.33 to 1.38 g cm^{-3} and the v_{trans} values over 0.07 km s^{-1} range, from 2.21 to 2.28 km s^{-1}. This means that the pressure–temperature path for producing HDAs determines its ρ and v_{trans} at 1.6 GPa and 77 K. A similar conclusion has been reached by examining the temperature and pressure derivatives of ρ and v_{trans}, and it has been further shown that the HDA formed by pressurizing LDA differs from the HDA formed by pressurizing ice Ih [37].

As mentioned earlier here, a variety of data from experiments performed by different groups, including some X-ray diffraction studies, have shown that the different temperatures of the ices Ih and Ic, the different pressurizing rates and the different time taken in performing the experiments produce different HDAs. Therefore, the term HDA is to be used in a generic sense referring to all high-density amorphous solids formed by the collapse of ices Ih and Ic, and not to a specific solid. It is also known [74] that the HDA formed at 77 K densifies by ∼5% when heated to 160 K at a pressure higher than 0.8 GPa, and we have found that the amorphization process is time-dependent, an aspect overlooked in studies in which conversion of LDA to HDA, and a further densified state of HDA has been achieved by pressurizing to 1.5 GPa at 125 K [153,154]. Our analysis has shown that there are complications in interpreting such further densification of HDA on increase in pressure as was done in Ref. [154]. To elaborate, the data for two states of HDA, one normally made and one densified, in Fig. 3 of Ref. [154] show that on cooling from 125 to 77 K, ρ of the densified HDA increases by ∼3.3% and ρ of undensified HDA by 2.3%, which makes expansion coefficient of the densified HDA as $\sim 7 \times 10^{-4}$ K^{-1}, which is ∼1.4 times as large as that of HDA. Such a high expansion coefficient value for a solid seems erroneous. For comparison, ρ of ice Ih increases from 0.9292 g cm^{-3} at 173 K to 0.9340 at 93 K [60], only by ∼0.55% over a larger temperature range, and at high temperatures, where the thermal expansion coefficient is relatively high. Also, their data [153,154] show that densified HDA has a higher (elastic) compressibility than HDA. Since these results are unexpected and appear counterintuitive, we suggest that the density data of HDA require experimental scrutiny before further discussion in terms of a pressure-induced distinct transformation of HDA to VHDA. As mentioned earlier here, recent wide angle diffraction and small angle neutron scattering studies of HDA and LDA [36] have shown that there is a correlation between their preparation conditions, microscopic structural properties, extent of heterogeneities on a mesoscopic spatial scale and transformation kinetics and further that there are only two modifications that can be identified as homogeneous disordered structures, namely VHDA and LDA, a finding consistent with the conclusion reached earlier on the basis of the thermal properties of HDAs and LDA [34,152].

7. Mechanism of pressure-amorphization

It is still uncertain whether ice Ih pressure collapses directly to a true amorphous solid, to an assembly of highly distorted crystals of no identifiable form, or to a random mixture of ice Ih and high pressure forms of ice that shows no crystal-like features in the X-ray and neutron diffraction. However, the term amorphous is used to distinguish solids showing no Bragg peaks from the crystal state, and for that reason the pressure collapsed ice Ih, which has shown no Bragg peaks has been pre-emptively called an amorph. The consequent use of the terms HDA and LDA has thus precluded discussion in terms of a collapsed state of an unknown structure. As mentioned earlier, the original explanation for amorphization of ice as a pressure-induced equilibrium melting at 0.5 GPa at 77 K may now be abandoned, because HDA used for construction of the phase diagram as reviewed in Ref. [44] was not an equilibrium state. This phase diagram construction has been questioned on the basis of a variety of studies even when the HDA formed was taken to be in an equilibrium state [83,157]. Also, the use of emulsions of ice for studying the

volume and enthalpy changes to determine the phase diagram of ice Ih and HDA has been shown to contain unresolved, extraneous thermodynamic effects that arise from interaction of the emulsifying agents with the ice surface [173].

We also recall that a mechanism based on Lindemann theory for melting applies to an ideal single crystal without point defects or lattice faults. Therefore, it is not expected to be valid for pressure collapse or amorphization of a polycrystalline sample which contains point defects, dislocations, internal strains and a large grain-boundary area, and whose amorphization pressure decreases, as described here, with decrease in the particle size. Also attempts to collapse single crystals of ice apparently have not succeeded [31]. In passing, we note that ice Ic seems to have a more defective structure than ice Ih, as indicated by a broader distribution of relaxation times [174], which can partly or, possibly, entirely explain the lower collapse pressure for ice Ic. Moreover, Lindemann melting is instantaneous, but pressure-amorphization has a slow kinetics that depends upon both T and p. As an alternative mechanism for pressure-amorphization, Sikka [175] has proposed that development of steric constraints in the crystal leads to its amorphization under pressure. In contrast, a recent high-resolution X-ray scattering study of the amorph formed by pressurizing ice Ih at 77 K to 1.8 GPa has shown that HDA has crystal-like inelastic response [86]. But phonon dispersion data obtained from an inelastic neutron diffraction study of single crystal of ice at 140 K hydrostatically compressed to 0.55 GPa by using fluid nitrogen as pressure transmitting medium [176], have led to the conclusion that already at 0.50 GPa pressure, a pronounced softening of the transverse acoustic phonon branch in the [100] direction and polarization in the hexagonal plane occurs [176]. This has been used to suggest that the lattice instability leads to amorphization of ice Ih already under 0.5 GPa pressure. Negative thermal expansion of inorganic crystals has also been considered as a requirement for their pressure collapse and to infer that such crystals would amorphize under pressure [177,178], and Strassle et al. [176] have used the negative expansion coefficient of ice Ih at low temperatures to determine its Born instability pressure as ∼2.5 GPa. This means that a single crystal of ice may amorphize at a pressure higher than 2.5 GPa, which is much higher than that observed here, and consistent with the finding that a single crystal of ice Ih did not amorphize at a hydrostatic pressure of ∼2 GPa [31]. Nevertheless, it is important to examine in these studies whether or not dissolution of nitrogen in ice Ih in experiments using fluid nitrogen as pressure transmitting medium [176], has an effect on the phonon dispersion data. Dissolved nitrogen at ambient pressure has been known to decrease the dielectrically measured molecular reorientation time of ice Ih by several orders of magnitude [179], and it is not certain whether it also has an effect on the temperature at which the expansion coefficient of pure ice is negative.

None of the above given mechanisms account for the observation that pressure-amorphization of ice Ih is time-dependent, with a well-defined kinetics, and with a distribution of times. Therefore, we consider other manners of melting that are peculiar to a polycrystalline sample as follows: at the grain-boundaries in a polycrystalline sample molecular or atomic arrangement is known to be liquid-like. It is also known that when a polycrystalline sample with submicron size crystals is heated in the temperature range far below its bulk melting point [180], significant premelting occurs at the three- and four-grain junctions of the crystallites. In this process, the change in the solid–liquid interfacial energy compensates for the change in the bulk energy, and thus in this incipient melting process, the melt and the solid remain at thermodynamic equilibrium. It is also known that the surface layer of ice crystals is disordered or water-like [113]. The amount of water contained in the grain boundaries and grain junctions of micron size grains in polycrystalline ice Ih at ambient pressure has been determined from both experiments [181] and calculations [180]. Since the relative ratio of the surface energy to bulk energy changes with change in pressure and temperature, this amount is expected to change with pressure. It is meaningful to recall that amorphization of ices Ih and Ic has been carried out by uniaxial loading at a rate of usually ∼0.1–0.2 GPa min^{-1} in most experiments, and uniaxial loading plastically deforms ice Ih crystallites anisotropically, thus converting the uniaxial load to a hydrostatic pressure presumably within less than 30 s at 77 K. As occurs generally for polycrystalline samples of materials, the ice crystallites reorient in this process, the sample recrystallizes, new grain-boundaries form and the population of the three- and four-grain junctions changes. This occurrence in turn would continuously change the incipient melting conditions at the grain junctions and grain boundaries, and although it is still the process of melting, it is not the same as the Lindemann melting.

There is no doubt that collapse of ices Ih and Ic leads to the filling of voids in their bulkier crystal structures, and this may be brought about if the Born [182] stability condition for their crystals is violated by the application of pressure. (Born had mathematically described the conditions for the loss of stability of an ideal crystal lattice, i.e., of a perfect single crystal. He had proposed that a crystal lattice becomes mechanically unstable when increase in the hydrostatic pressure softens the transverse acoustic phonon modes and the elastic modulus decreases and the collapse occurs homogeneously throughout the crystal lattice. This leads to the formation of another crystal phase.) The collapse pressure is determined by the manner in which the elastic constants change on compression. Although Born had considered the lattice stability violation conditions for the phase transformation of one crystal to another, and not for transformation of a crystal to amorphous solid, which was not known at the time, his theory has been used to calculate [183], in a quasi-harmonic approximation, the mechanical collapse pressure of an ideal ice Ih single crystal at different temperatures. But this seems irrelevant to polycrystalline ices Ih and Ic, which contains grain boundaries and three- and four-grain junctions in which impurities segregate, and its individual crystals contain point defects, impurities, and dislocations. Moreover, the state of the crystals in a polycrystalline mass change as uniaxial loading plastically deforms the ice sample, causes its crystal grains to reorient, dislocations population to increase and the dislocations to move. All of these features, which are characteristic of a sample as well as that of a material, are expected to alter the Born instability (or stability violation) pressure and thereby cause the

extent of amorphization to depend upon the time, temperature and pressure, and to a small degree upon the microstructure of the sample itself. It has also been found that dislocations in a single crystal of ice have an extended noncrystalline core [184], which also would alter the conditions of pressure-amorphization. Thus it may seem that pressure-amorphization of ice Ih and ice Ic involves two mechanistically distinct processes: (i) incipient melting at the inter-granular regions in a polycrystalline sample and (ii) increase in the population of dislocation cores containing disordered arrangements of water molecules in the crystallites. It should also be noted that the much lower pressure of LDA to HDA conversion cannot be explained by the influence of defects and their diffusion on the Born instability condition of LDA, even though in terms of decrease in κ LDAs collapse is similar to that of ices Ih and Ic.

In a mechanical collapse resulting from the Born stability violation in a crystal, lattice faults would lower the collapse pressure, because these faults store energy and in most cases lower the crystal's density from that of an ideal lattice. More importantly, a variation in the population of the lattice faults would cause different crystallites in the sample to collapse at different pressures. Thus one would expect a distribution of the Born instability pressures (of different crystallites) in a polycrystalline sample, which would broaden the pressure range for the mechanical collapse of the sample. Hence even at a very slow compression rate, full amorphization would be reached only after the pressure is of a magnitude high enough to collapse the near ideal ice crystal of the highest Born instability pressure. (The situation may be seen as analogous to a multi-component crystalline composite, in which each component would collapses at its own characteristic pressure.) If this occurred then ice would coexist with the amorph at formally infinite annealing time. This means that the final state achieved would remain a mixture of (stronger) ice Ih crystallites that did not collapse at a given pressure and the amorph that formed by the collapse of (weaker) ice crystallites. This would also explain the observation that the onset pressure of amorphization decreases with decrease in the crystal grain size in the sample [31].

Electrostatic interactions in the structure of crystalline ices have been found to be co-operative in nature [185,186], with the consequence that breaking of some H-bonds weakens the strength of the others. Accordingly, breaking of some H-bonds as a result of structural collapse of ices Ih and Ic would weaken the neighbouring H-bonds in the ice crystal. If that were to occur, subsequent pressure-amorphization of ice would become easier, i.e., after part of the ice Ih structure has collapsed, further collapse would require a smaller increase in pressure. But the stretched sigmoid shape plots of volume, thermal conductivity and high-frequency permittivity against pressure have shown that this weakening effect is inconsequential. Therefore, the regions in which the structure collapses seem to be small enough in size as not to cause a sudden and rapidly increasing collapse of the whole crystal. Thus although the Born criterion for crystal stability may remain valid for the mechanical collapse of ice, its manifestation is altered by a distribution of the mechanical collapse pressures in a polycrystalline mass. Nevertheless, the time-dependent pressure-amorphization of ice Ih at a given p–T condition may be reconciled with Born's stability criterion if occurrence of another molecular process that changes the crystallite's microstructure is included. On the basis of our knowledge of plastic deformation of polycrystalline sample and concurrent recrystallization, we suggest that this molecular process would be diffusion of defects, redistribution of impurities and dislocations and partial melting. This mechanism would continuously alter, with time, the distribution of the collapse pressure at a given p–T condition.

Whether or not this collapse would produce highly distorted ice Ih crystals or extremely small, nanometer size crystals of high-pressure forms of ices are yet to be investigated in detail. We note that formation of ultraviscous water [53,54] on heating the pressure collapsed state does not conflict with the view that its structure may contain highly distorted and/or nanocrystals of high-pressure ices because, (i) the melting point of such crystals would be significantly lower than of large crystals, as given by the Gibbs–Thomson equation, and (ii) such crystals may transform to the lower energy glassy state in the same manner as mechanically amorphized states do on heating by loss of enthalpy.

Without referring to the nature of the product, we conclude that the collapse onset pressure, the pressure-range for complete amorphization and the characteristic amorphization time at a given p–T condition are determined by at least five effects that are intrinsic to an ice Ih sample: (i) the rate of plastic deformation of crystallites and their recrystallization under a uniaxial stress, (ii) the concentration of lattice faults in the crystallites, (iii) the Born instability pressure of the crystallites and the distribution of this pressure, (iv) the redistribution of impurities and dislocations and partial melting during the period of amorphization, and (v) the pressurizing rate. It is conceivable that in Johari's experiment mentioned in Ref. [31], a single crystal of ice Ih at 77 K did not amorphize at pressures of up to 2 GPa because the Born instability pressure for a single large crystal, which may be calculated in a harmonic approximation, could be higher than for a polycrystalline sample, and this pressure was not reached in his experiment [31]. On the opposite end, it is conceivable that crystals of ice approaching several nanometers in size may amorphize at a pressure as low as 0.1 GPa. This may be tested by an experiment in which change in properties from nanocrystal state to amorphous state may be detected.

8. Thermodynamics and kinetics of pressure collapsed amorph and of ultraviscous water

Amorphous states of a material made by different techniques have different properties. We recall that a glass is formed only by cooling a liquid or by compressing a liquid. The occurrence is usually reversible on cooling and heating, although the cooling path in a temperature plane differs from the heating path as a result of different extents of structural relaxation during the time taken to cool the liquid or heat the glass. In those cases when a liquid cannot be supercooled by usual methods, the glass has to be formed by hyperquenching the liquid, i.e., by cooling at a rate higher than 10^5 K s^{-1}, as in the case of water [23]. The glass thus produced has a high fictive temperature, T_f, than a glass formed

by cooling of a liquid, say at 0.1 K s^{-1}. The structure of a hyperquenched glass relaxes with time to a lower energy state of lower T_f at a rate that increases with increase in the temperature. (For a discussion of the subject, see for example Ref. [164].) When such a glass is heated, its energy and T_f decrease. After its state has crossed the equilibrium liquid line in the temperature plane for a certain heating rate, its energy and T_f increase, the glass softens and becomes an ultraviscous liquid. If the liquid crystallizes rapidly, the glass-softening to ultraviscous liquid may be immediately followed by the latter's crystallization and may not be observed if crystal nuclei had already formed as a result of the heat released during structural relaxation [119]. For a material that does not crystallize in the ultraviscous state, this process is illustrated in Fig. 11(A).

In contrast to the normal supercooling of a liquid, a variety of technologically useful amorphous solids are made by [91], (i) vapour-deposition on a cold substrate, (ii) rapid evapouration of a solution, (iii) chemical reaction that leaves a solid product, (iv) electrodeposition and (v) mechanical deformation of crystals in a high speed ball-mill. The internal energy, entropy and T_f of these solids are much higher than those of glasses formed by normal cooling. When heated, their structure rapidly relaxes to a lower energy amorphous structure [91]. Further heating mechanically softens the solid slowly and it ultimately becomes an ultraviscous liquid, which may crystallize rapidly and may therefore not show, in some cases, the characteristic glass-softening endotherm [91]. The thermodynamic path along which these changes occur is irreversible, but it is cyclic in as much as the final amorphous solid can be converted back to the original states of vapour, solution, chemical reactants, crystal, etc.

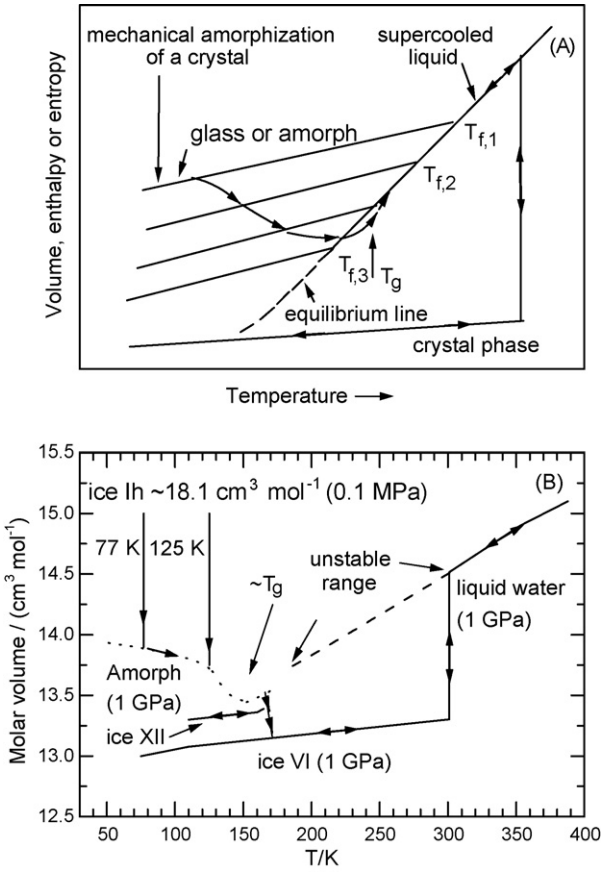

Fig. 11. (A) An illustration for the formation of high-energy amorphs of high fictive temperatures by mechanical deformation, and/or by rapid cooling. The spontaneous structural relaxation in a heating rate dependent manner to a low fictive temperature, low energy state and then glass transition are indicated by arrows. In this case the ultraviscous liquid does not crystallize. (B) Pressure collapse of ice Ih, its structural relaxation to a denser, low thermal conductivity solid with time and on heating, its gradual transformation to an ultraviscous liquid which crystallizes to ice XII on fast heating and finally to ice VI. The segments of the plots are labelled and arrows are used to show the direction of change.

We propose that in terms of its high energy, the pressure collapsed state of ices Ih and Ice is qualitatively similar to the amorphous state produced by mechanical deformation of crystals, to the glassy state formed by hyperquenching of a liquid, or to the amorphous state formed by vapour-deposition. In the illustration of Fig. 11(A), the mechanically deformed amorphous solid produced by mechanical deformation of crystals is shown to have a high internal energy, as for mechanically amorphized metal crystals and organic crystals [187,188]. The self-diffusion in the mechanically deformed solids is much faster than in their undeformed state. Thermodynamically, the basic difference between a mechanically amorphized crystal state and the amorph formed by pressure collapse of ices Ih and Ic is that the mechanically amorphized state is bulkier than the parent crystal, and the amorph formed by pressure collapse of these two ices is denser than the parent crystals, which do not survive a pressure higher than 0.8 GPa. But, as the amorph is bulkier than ice VI, which is the stable crystal phase at the collapse-pressures of ices Ih and Ic, the density of the pressure collapsed state should be compared with the density of ice VI. In earlier discussion of the properties of the amorph at ambient pressure and 77 K, this aspect has been unfortunately overlooked. It remains to be seen whether an amorph of lower density than ice VI can be produced by mechanical deformation of ice VI at 1 GPa, or else produced by mechanical deformation of recovered ice VI at ambient pressure and 77 K, by using a high-speed ball mill in the same manner as used for ordinary crystals [189].

To illustrate the pressure-amorphization of ices Ih and Ic, the structural relaxation of the solid on heating and the conversion of the relaxed state to ultraviscous water, we have plotted the molar volume of these various states against the temperature in Fig. 11(B). In this figure, ices Ih and Ic have molar volume of ~18.1 ml mol^{-1} and they collapse to a solid of 13.8 ml mol^{-1} volume at ~1 GPa at 77 K, and to 13.75 ml mol^{-1} volume at 125 K. The collapsed state becomes denser on heating according to a temperature-dependent rate, and after the equilibrium line has been crossed on heating, the volume increases. Further heating transforms it to ultraviscous water whose dielectric relaxation time is ~1 s at 140 K [53]. On further heating to 150–160 K range, the ultraviscous water may crystallize to ice XII, which exists in the 0.7–1.5 GPa and 158–212 K range, but also the resulting crystalline phase may depend upon the heating rate [84,190]. Ice XII can be thermally cycled at 1 GPa pressure along the path shown by the oppositely pointing arrows. (Note that crystallization has been found to occur also to mix-

tures of ices VI and XII [8] and mixtures of ices IV and XII [84], and therefore there is some ambiguity of crystallization in this metastable state). On heating, metastable ice XII transforms to the stable phase ice VI [190] at 1 GPa as is indicated in Fig. 11(B). Ice VI can be heated at 1 GPa and it melts to water at a temperature slightly above 300 K. Studies of the liquid ice VI phase boundary have shown that liquid water does not supercool through the ice VI stability region and water at 1 GPa in the 300–140 K range is unstable. It seems now, however, that water's ultraviscous state at high pressure can be obtained *via* the pressure collapse route of ice Ih, as inferred from the plot of volume in Fig. 11(B). We also note that the plots of enthalpy against temperature of these phases would show the same features as the volume, with all points of transformation remaining the same as for the plots in Fig. 11(B).

One may argue that contrary to the above-given postulates, heating of the microcrystalline or submicrocrystalline particles of the various ices formed by pressure-amorphization would cause them to act as a nuclei for crystal growth and would not melt them to an ultraviscous liquid. While this may be true in some cases, it is well known that mechanical pulverization or comminution of organic, inorganic and metallic crystals in high-speed ball mills creates micron and submicron size particles with a large population of point defects and dislocations and these particles become brittle. As the volume to surface area is already large and the surface tension of the particles is different from that of the usual crystal-nuclei formed in the equilibrium conditions, these particles do not act as sites for crystal growth. Instead the mechanically amorphized powder of highly strained particles converts to a glassy state which on heating shows a T_g-endotherm in the DSC scan, immediately after a broad exothermic feature. For example, mechanically amorphized 1,3,5-tri-α-naphthylbenzene studied by Yamamuro et al. [191], and discussed in connection with high enthalpy amorphous solids [91], and a number of pharmaceuticals [187,188,192] have clearly shown conversion of mechanically deformed crystallites to glasses. It is also a well-recognized occurrence in the packaging technology of pharmaceuticals. More recently, Bhat et al. [193] have shown that ball-milled crystalline particles of $PbGeO_3$ become amorphous and show a T_g-endotherm on heating in the same manner as a number of other materials have shown. Therefore, it would not be a unique case for the highly distorted micron or submicron crystals of the ices to become a glass or ultraviscous liquid rather than to grow to larger crystals. It is conceivable that the surface tension of such mechanically deformed particles differs substantially from the interfacial tension used in the nucleation and crystal growth theories and therefore those theories may not be applicable here. Once the viscosity of the liquid decreases on heating to $T > T_g$, new crystals nucleate and grow at a rate that depends upon the viscosity of the liquid and the liquid crystallizes, as illustrated by the paths shown in Fig. 11(A) and (B) for water at high pressures.

9. Summary and concluding remarks

Thermal conductivity of the ices shows a remarkable variety of unexpected behaviours: It is lowest for an ice clathrate, and not for the water's amorphous solids, an apparently amorphous solid of low-density, LDA, shows a crystal-like temperature dependence of thermal conductivity and a distinctly crystalline ice clathrate a glass-like temperature dependence. Crystals and amorphous solids of water of higher density may have a lower thermal conductivity, and two crystal forms of the same density and properties, ices Ih and Ic, show unexpectedly different thermal conductivities.

The observed variation of thermal conductivity and heat capacity of the high-density amorphous solid with pressure may be qualitatively explained by the Debye theory. A quantitative analysis of the heat capacity shows that the frequency of phonon modes increases and the Debye energy and the anharmonicity decrease. While the Debye phonons can explain the decrease in the heat capacity of HDA by $\sim$5% GPa^{-1}, and also the increase in the thermal conductivity towards a plateau value, they do not quantitatively describe the increase in thermal conductivity within the approximation of a constant phonon scattering strength.

The states of as-made vapour-deposited amorphous solid water (ASW) and hyperquenched glassy water (HGW) have a high energy and high fictive temperature, and both show a prominent enthalpy decrease due to structural relaxation on heating. This decrease masks the onset of glass-softening endotherm before the ultraviscous liquid begins to crystallize rapidly to ice Ic. Removal of this heat by isothermal annealing prior to heating reveals this endotherm and yields a T_g of 136 K for the glassy state of water. LDA also shows enthalpy decrease due to structural relaxation but it is relatively less and its T_g is 129 K. The isotope effect on T_g and a variety of thermodynamic, vibrational and diffraction features have shown that glassy water, and the ultraviscous water obtained by heating it, are different from LDA and its high temperature state. Thus, there is no evidence that the two states of liquid water, one formed by heating HDA and the other formed by heating ASW and HGW, are the same.

The dielectric relaxation time of ultraviscous water at ambient pressure is estimated to be 30 s at 140 K [118,119] and of water formed on heating HDA at 1 GPa and 130 K is determined as 5 s [53,54]. The dielectric relaxation time of LDA is more than 10 times of that for HDA at 0.3 GPa and 130 K [110]. Thus T_g of the higher density state of water at 1 GPa is lower than the T_g of lower density state at ambient pressure. The increase in relaxation time at the HDA to LDA transition, despite the 25% density decrease, is likely due to a change in structure to one which obeys the ice rules [110]. This explains the much restricted dipolar mobility in LDA as it does also in (the proton-disordered) ices Ih and Ic. An LDA structure that obeys the ice rules would also explain the large isotope effect on the T_g of LDA [111].

The crystal structures of polycrystalline ice Ih and ice Ic collapse at a pressure greater than 0.7 GPa at a rate that varies with the temperature, pressure and crystal size. The pressurizing rate, the temperature and the period of sustained pressure all have an effect on the structure and properties of the high-density amorphous solid formed by the collapse of ice. Thus the study of the samples of the so-called HDA refers to the study of a generic state of high-density and not to a specific structure or properties of a solid. As the temperature is increased, the pressure for structural

collapse becomes less, an effect opposite to that observed for vitrification of liquids for which vitrification pressure increases as the temperature is increased. This pressure is lower for ice Ic than for ice Ih, and it is also lower when the ice crystal size is in the micron range. Therefore, the collapse-pressure is increased when thermal energy of ice is low, and decreased when surface energy of ice is high. Thus, for a given collapse-pressure there is a thermal energy equivalence for the surface energy, and it is expected that samples with crystal-grain size approaching nanometer scale would (collapse) amorphize at a much lower pressure than 0.7 GPa. As the nanometer size crystals would be difficult to distinguish from an amorphous solid by diffraction measurements, changes in volume and thermal conductivity on increase in pressure would need to be used for such studies.

The kinetics of pressure-amorphization of ice Ih has a distribution of time constants that is expressed in terms of the stretched exponential parameter. The broad pressure range and the time-, the temperature-, and the pressure-dependences of structural collapse that leads to amorphization can be reconciled with Born's theory of mechanical collapse, by transverse phonons softening, only if the effects of lattice faults (point defects, dislocations) and of internal surfaces are included. A single crystal of ice Ih may collapse at a much higher pressure than a polycrystalline sample.

Such effects may also be observable for other hydrogen-bonded crystals, e.g., resorcinol [194] and α-hydroquinone [195] whose Raman spectra have shown gradual loss of crystal-like features with increase in pressure above a certain pressure. It would be important to recover the collapsed organic crystals at ambient pressure and examine their structural disorder and to study their thermal properties at ambient pressure to determine if they also form a high-density and a low-density amorph. Detailed studies of pressure collapse of polycrystalline samples as a function of the crystal grain size may generally lead to a better understanding of the role of the sample's surface energy relative to its internal energy. It may also help understand the merits of the Born's theory of crystal-instability, especially if the Born-instability view is to be extended to pressure-amorphization of crystals. It may also be important to determine if such crystals can be mechanically amorphized in a high-speed ball mill at ambient pressure and then to investigate the nature of the amorph formed. Real-time studies by diffraction, Raman and FTIR spectroscopy methods during a crystal's collapse isothermally at a fixed pressure, as well as with slowly increasing pressure, would be required for understanding how the amorphous state is achieved by pressurizing crystals. This is particular important because pressure collapsed crystals are in a high-energy state and in this state they behave like mechanically amorphized crystals. After spontaneous relaxation at a relatively high temperature to a lower energy disordered state, they become analogous to the hyperquenched glassy state and show a glass-softening range.

The collapsed state on heating itself may yield new crystal forms, as in the formation of ice XII [196], and new crystal forms of some materials may be technologically useful. The pressure collapsed state of ice Ih at 1 GPa structurally relaxes rapidly on heating and the solid at 1 GPa becomes ultraviscous water at ∼140 K. On further heating at 1 GPa, this water crystallizes first to the denser ice XII [84,190] and then to ice VI [190], or, in certain heating conditions, to a mixture of ices XII and VI [8] or to a mixture of ices XII and IV [84]. Thus the amorphous solid at 1 GPa is bulkier than ice VI, its stable crystal phase. It is conceivable that high-speed ball-milling of ice VI at temperatures below 130 K at 1 GPa may mechanically amorphize it to a high-density amorph in the same manner as ordinary crystals are amorphized. Alternatively, recovered ice VI at ambient pressure and 77 K may be amorphized by ball-milling to obtain the same state as that obtained by pressure collapse of ices Ih or Ic. The ultraviscous water at 1 GPa, which is difficult to obtain by supercooling water at 1 GPa, can be obtained *via* the pressure collapse of ice Ih.

Since 2004, a number of new findings, particularly those regarding the pressure, temperature and time dependence of pressure-amorphization of ice Ih, have now confirmed that there is a mesoscopic heterogeneity in the HDAs produced by different methods. Moreover, it has been concluded that there are only two homogeneous amorphous solids, one is LDA and the second is the so-called VHDA. It has also been shown that the HDA produced by pressurizing LDA differs from the HDA produced by pressurizing ice Ih [37], and X-ray diffraction of HDA produced from ice Ic differs from that produced from ice Ih [197]. Also, different states of HDAs, more precisely distinguished from diffraction studies, have been produced by annealing a state of HDA at ∼0.2 GPa and by thermally cycling the samples [198]. A study of pressurized and annealed tetrahydrofuran ice clathrate (produced by pressurizing to 1.5 GPa at 77 K, heating the densified sample to 150 K for annealing and finally recovering at ambient pressure at 77 K) has shown that its Raman spectra at 25 K and its X-ray diffraction are similar to those for HDA [199]. These observations indicate the need for controlling the temperature–pressure–time profile in producing the pressure collapsed state of reproducible properties, as well as for care in comparing impure samples against pure HDAs. Nevertheless, they confirm that HDA refers to a generic state and not to a specific solid [37].

A variety of high-pressure crystalline phases of ice are formed when the collapsed state of ice produced at different pressures and temperatures is heated at different (fixed) high pressures [8,84]. These metastable crystalline phases are "intruders" as they are produced in the pressure–temperature stability domain of other high-pressure crystalline ices, and they persist at low temperatures. For example, ice XII, a mixture of ices VI and XII and a mixture of ices IV and XII, all form in the domain of ice VI. These "intruders" would ultimately transform to the stable crystalline phase by a thermally activated kinetics. It should be noted that some of these crystalline ice phases and their mixtures at high pressures and low temperatures have the same density as one of the HDAs, but their phonon properties are expected to be different.

Crystallization on heating of the pressure collapsed state of ice Ih to a multiplicity of high-pressure phases of ice is still not understood. As a consequence, the nature of the pressure collapsed state is debated, as to whether it is a composite of the high-pressure phases of ice at a mesoscopic scale, some of

which may preferentially grow into larger crystals at certain pressure and temperature conditions and thus appear to produce "intruder" phases in the stability domain of other ices, or is it a true amorphous solid in which no two water molecules have identical environment and whose random crystallization produces different "intruder" phases. Here information obtained from pressure collapse of crystals without water-like tetrahedral hydrogen bonding would reveal not only the mesoscopic scale character of the pressure collapsed solids in general, but also that whether the formation of low-, and the high-density amorphs is a natural consequence of pressure collapse or is there just a continuity of disordered solids of varying densities between the two extremes of low and high densities, as would be achieved by compressing a liquid at different pressures and then supercooling it. Such studies may also help determine whether pressure collapse and subsequent formation of different amorphs is general enough to be understood as a phenomenon in terms of changes in the intermolecular forces, or whether it is a feature resulting from plastic deformation of the crystal grains in a polycrystalline sample.

Acknowledgements

GPJ is grateful to NSERC of Canada for a general research grant. OA is grateful for financial support from the Swedish Research Council.

References

[1] V.F. Petrenko, R.W. Whitworth, Physics of Ice, Oxford University Press, Oxford, 1999.
[2] C.G. Salzmann, A. Hallbrucker, J.L. Finney, E. Mayer, Phys. Chem. Chem. Phys. 8 (2006) 3088.
[3] C.G. Salzmann, A. Hallbrucker, J.L. Finney, E. Mayer, Chem. Phys. Lett. 429 (2006) 469.
[4] A. Polian, M. Grimsditch, Phys. Rev. Lett. 52 (1984) 1312.
[5] G.P. Johari, J. Chem. Phys. 122 (2005) 194504.
[6] H. Engelhardt, E. Whalley, J. Chem. Phys. 56 (1972) 2678.
[7] C. Lobban, J.L. Finney, W.F. Kuhs, Nature 391 (1998) 268.
[8] S. Klotz, G. Hamel, J.S. Loveday, R.J. Nelmes, M. Guthrie, Z. Kristallogr. 218 (2003) 117.
[9] J.D. Bernal, R.H. Fowler, J. Chem. Phys. 1 (1933) 515.
[10] M. von Stackelberg, H.R. Müller, Z. Electrochem. 58 (1954) 25.
[11] D.W. Davidson, in: F. Franks (Ed.), Water—A comprehensive Treatise, vol. 2, Plenum, New York, 1973, p. 115 (Chapter 3).
[12] J.A. Ripmeester, J.S. Tse, C.I. Ratcliffe, B.M. Powell, Nature (London) 325 (1987) 135.
[13] Y.F. Makogon, in: translated by W.J. Cieslewicz (Ed.), Hydrates of Natural Gases, PennWell, Tulsa, 1981.
[14] B. Berecz, M. Bolla-Achs, Gas Hydrates—Studies in Inorganic Chemistry, vol. 4, Elsevier, Amsterdam, 1983.
[15] E.D. Sloan, Clathrate hydrates of Natural Gases, 2nd ed., Marcel Dekker, New York, 1998.
[16] W.L. Mao, H.-K. Mao, A.F. Goncharov, V.V. Struzhkin, Q. Guo, J. Hu, J. Shu, R.J. Hemley, M. Somayazulu, Y. Zhao, Science 297 (2002) 2247.
[17] L.J. Florusse, C.J. Peters, J. Schoonman, K.C. Hester, C.A. Koh, S.F. Dec, K.N. Marsh, E.D. Sloan, Science 306 (2004) 469.
[18] H. Lee, J.-W. Lee, D.Y. Kim, J. Park, Y.-T. Seo, H. Zeng, I.L. Moudrakovski, C.I. Ratcliffe, J.A. Ripmeester, Nature 434 (2005) 743.
[19] F. Schüth, Nature 434 (2005) 712.
[20] G.P. Johari, La Recherche 387 (2005) 25.
[21] E.F. Burton, W.F. Oliver, Proc. Roy. Soc. (Lond.) Ser. A 153 (1935) 166.
[22] J.A. McMillan, S.C. Los, Nature (London) 206 (1965) 806.
[23] E. Mayer, J. Appl. Phys. 58 (1985) 663.
[24] E. Mayer, J. Phys. Chem. 89 (1985) 3474.
[25] G.P. Johari, A. Hallbrucker, E. Mayer, Nature (London) 330 (1987) 552.
[26] A. Hallbrucker, E. Mayer, G.P. Johari, J. Phys. Chem. 93 (1989) 4986.
[27] O. Mishima, L.D. Calvert, E. Whalley, Nature (London) 310 (1984) 393.
[28] O. Mishima, L.D. Calvert, E. Whalley, Nature (London) 314 (1985) 76.
[29] G.P. Johari, A. Hallbrucker, E. Mayer, J. Phys. Chem. 94 (1990) 1212.
[30] O. Mishima, J. Chem. Phys. 100 (1994) 5910.
[31] G.P. Johari, Phys. Chem. Chem. Phys. 2 (2000) 1567.
[32] E.L. Gromnitskaya, O.V. Stal'gorova, V.V. Brazhkin, Phys. Rev. B 64 (2001) 094205.
[33] O. Andersson, A. Inaba, Phys. Chem. Chem. Phys. 7 (2005) 1441.
[34] G.P. Johari, O. Andersson, J. Chem. Phys. 120 (2004) 6207.
[35] G.P. Johari, O. Andersson, Phys. Rev. B 73 (2006) 094202.
[36] M.M. Koza, T. Hansen, R.P. May, H. Schober, J. Non-Cryst. Solids 352 (2006) 4988.
[37] G.P. Johari, J. Chem. Phys. 121 (2004) 8428.
[38] A.G.G.M. Tielens, L.J. Allamandola, in: G.E. Morfill, M. Scholer (Eds.), Physical Processes in Interstellar Clouds, Reidel, Dordrecht, 1987, p. 223.
[39] J.M. Greenberg, in: J.M. Greenberg, V. Pironell (Eds.), Chemistry in Space, Kluwer Academic, Dorderecht, Netherlands, 1991, p. 227.
[40] M.C. Festou, H. Rickman, R.M. West, Astron. Astrophys. Rev. 5 (1993) 37.
[41] M.J. Mumma, P.R. Weissman, S.A. Stern, in: E.H. Levy, J.I. Lunine, M.S. Matthews (Eds.), Protstars and Planets III, Univ. of Arizona Press, Tucson, 1993, p. 1177.
[42] P. Jenniskens, D.F. Blake, Science 265 (1994) 753.
[43] P. Jenniskens, D.F. Blake, M.A. Wilson, A. Pohorille, Astrophys. J. 455 (1995) 389.
[44] P.G. Debenedetti, J. Phys. Condens. Matter 15 (2003) R1669.
[45] R.G. Ross, P. Andersson, G. Bäckström, Nature (London) 259 (1976) 553.
[46] R.G. Ross, P. Andersson, G. Bäckström, High Temp.-High Press. 9 (1977) 87.
[47] R.G. Ross, P. Andersson, G. Bäckström, J. Chem. Phys. 68 (1978) 3967.
[48] O. Andersson, H. Suga, Phys. Rev. B 50 (1994) 6583.
[49] O. Andersson, G.P. Johari, H. Suga, J. Chem. Phys. 120 (2004) 9612.
[50] O. Andersson, H. Suga, Phys. Rev. B 65 (2002) 140201.
[51] B. Håkansson, P. Andersson, G. Bäckström, Rev. Sci. Instrum. 59 (1988) 2269.
[52] H.S. Carslaw, J.C. Jaeger, Conduction of Heat in Solids, 2nd ed., Clarendon, Oxford, 1959, p. 341.
[53] O. Andersson, Phys. Rev. Lett. 95 (2005) 205503.
[54] O. Andersson, A. Inaba, Phys. Rev. B 74 (2006) 184201.
[55] H. Forsman, J. Phys. D: Appl. Phys. 22 (1989) 1528.
[56] G.P. Johari, S.J. Jones, Philos. Mag. 54 (1986) 311.
[57] G.P. Johari, E. Whalley, J. Chem. Phys. 64 (1976) 4484.
[58] G.P. Johari, E. Whalley, J. Chem. Phys. 115 (2001) 3274.
[59] O. Andersson, B. Sundqvist, G. Bäckström, High Press. Res. 10 (1992) 599.
[60] D. Eisenberg, W. Kauzmann, The Structure and Properties of Water, Oxford University Press, Oxford, UK, 1969.
[61] A.I. Krivchikov, B.Ya. Gorodilov, O.A. Korolyuk, V.G. Manzhelii, O.O. Romantsova, H. Conrad, W. Press, J.S. Tse, D.D. Klug, Phys. Rev. B 73 (2006) 064203.
[62] R.G. Ross, P. Andersson, B. Sundqvist, G. Bäckström, Rep. Prog. Phys. 47 (1984) 1347.
[63] R. Berman, Thermal Conduction in Solids, Clarendon, Oxford, 1976.
[64] N.W. Ashcroft, N.D. Mermin, Solid State Physics, Saunders College Publishing, Philadelphia, 1976, p. 258, 501.
[65] O. Andersson, PhD Thesis, Umeå University, Umeå, 1991.
[66] H. Suga, T. Matsuo, O. Yamamuro, Pure Appl. Chem. 64 (1992) 17; H. Suga, T. Matsuo, O. Yamamuro, Supramol. Chem. 1 (1993) 221.
[67] O. Andersson, H. Suga, J. Phys. Chem. Solids 57 (1996) 125.
[68] P. Andersson, R.G. Ross, J. Phys. C 16 (1983) 1423.
[69] J.S. Tse, M.A. White, J. Phys. Chem. 92 (1988) 5006.

[70] J.S. Tse, V.P. Shpakov, V.R. Belosludov, F. Trouw, Y.P. Handa, W. Press, Europhys. Lett. 54 (2001) 354.
[71] R.G. Ross, P. Andersson, G. Bäckström, Nature (London) 290 (1981) 322.
[72] J.L. Cohn, G.S. Nolas, V. Fessatidis, T.H. Metcalf, G.A. Slack, Phys. Rev. Lett. 82 (1999) 779.
[73] O. Andersson, G.P. Johari, J. Chem. Phys. 121 (2004) 3936.
[74] T. Loerting, C. Salzmann, I. Kohl, E. Mayer, A. Hallbrucker, Phys. Chem. Chem. Phys. 3 (2001) 5355.
[75] R.O. Pohl, J. Non-Cryst. Solids 352 (2006) 3363.
[76] X. Yu, D.M. Leitner, J. Chem. Phys. 123 (2005) 104503.
[77] J. Klinger, Science 209 (1980) 271.
[78] Y.P. Handa, D.D. Klug, J. Phys. Chem. 92 (1988) 3323.
[79] W.F. Giauque, J.W. Stout, J. Am. Chem. Soc. 58 (1936) 1144.
[80] D.D. Klug, C.A. Tulk, E.C. Svensson, C.-K. Loong, Phys. Rev. Lett. 83 (1999) 2584.
[81] A.I. Kolesnikov, J. Li, S.F. Parker, R.S. Eccleston, C.-K. Loong, Phys. Rev. B 59 (1999) 3569.
[82] H. Schober, M.M. Koza, A. Tölle, C. Masciovecchio, F. Sette, F. Fujara, Phys. Rev. Lett. 85 (2000) 4100.
[83] G.P. Johari, J. Chem. Phys. 112 (2000) 8573.
[84] C.G. Salzmann, E. Mayer, A. Hallbrucker, Phys. Chem. Chem. Phys. 6 (2004) 5156.
[85] D. Minceva-Sukarova, W.F. Sherman, G.R. Wilkinson, J. Phys. C: Solid State Phys. 17 (1984) 5833.
[86] M.M. Koza, H. Schober, B. Geil, M. Lorenzen, H. Requardt, Phys. Rev. B 69 (2004) 024204.
[87] D.D. Klug, E. Whalley, E.C. Svensson, J.H. Root, V.F. Sears, Phys. Rev. B 44 (1991) 841.
[88] K. Röttger, A. Endriss, J. Ihringer, S. Doyle, W.F. Kuhs, Acta Cryst. B 50 (1994) 644.
[89] O. Andersson, A. Inaba, J. Chem. Phys. 122 (2005) 124710.
[90] A.J. Leadbetter, Proc. R. Soc. Lond., Ser. A 287 (1965) 403.
[91] G.P. Johari, J. Phys. Chem. B 107 (2003) 9063.
[92] E. Mayer, in: M.C. Bellissent-Funel, J.C. Dore (Eds.), Hydrogen-bonded Networks, Kluwer, Dordrecht, 1994, pp. 355–372.
[93] I. Kohl, L. Bachmann, A. Hallbrucker, E. Mayer, T. Loerting, Phys. Chem. Chem. Phys. 7 (2005) 3210.
[94] A. Kouchi, T. Kuroda, Nature (London) 344 (1990) 134.
[95] M.H. Moore, R.L. Hudson, Astrophys. J. 401 (1992) 353.
[96] G.A. Baratta, G. Leto, F. Spinella, G. Strazzulla, G. Foti, Astron. Astrophys. 252 (1991) 421.
[97] S. Klotz, J.M. Besson, G. Hamel, R.J. Nelmes, J.S. Loveday, W.G. Marshall, Nature 398 (1999) 681.
[98] A. Hallbrucker, E. Mayer, J. Phys. Chem. 91 (1987) 503.
[99] M. Sugisaki, H. Suga, S. Seki, Bull. Chem. Soc. Jpn. 41 (1968) 2591.
[100] G.P. Johari, J. Chem. Phys. 116 (2002) 8067.
[101] S. Ram, G.P. Johari, Philos. Mag. B 61 (1990) 299.
[102] G.P. Johari, J. Chem. Phys. 102 (1995) 6224.
[103] E. Mayer, J. Microsc. 160 (1985) 3.
[104] A. Hallbrucker, E. Mayer, G.P. Johari, J. Phys. Chem. 93 (1989) 7751.
[105] G.P. Johari, J. Mol. Struct. 528 (2000) 249.
[106] G.P. Johari, M. Beiner, C. Mcdonald, J. Wang, J. NonCryst. Solids 278 (2000) 58.
[107] G.P. Johari, Chem. Phys. 258 (2000) 277.
[108] K. Hofer, G. Astl, E. Mayer, G.P. Johari, J. Phys. Chem. 95 (1991) 10777.
[109] K. Hofer, A. Hallbrucker, E. Mayer, G.P. Johari, J. Phys. Chem. 93 (1989) 4674.
[110] O. Andersson, Phys. Rev. Lett. 98 (2007) 57602.
[111] G.P. Johari, A. Hallbrucker, E. Mayer, J. Chem. Phys. 95 (1991) 6849.
[112] G.P. Johari, A. Hallbrucker, E. Mayer, J. Chem. Phys. 92 (1990) 6742.
[113] P.V. Hobbs, Ice Physics, Clarendon, Oxford, 1974.
[114] G.P. Johari, A. Hallbrucker, E. Mayer, J. Chem. Phys. 95 (1991) 2955.
[115] G.P. Johari, A. Hallbrucker, E. Mayer, J. Chem. Phys. 97 (1992) 5851.
[116] W. Hage, A. Hallbrucker, G.P. Johari, E. Mayer, J. Chem. Phys. 100 (1994) 2743.
[117] W. Hage, A. Hallbrucker, G.P. Johari, E. Mayer, J. Chem. Phys. 103 (1995) 545;
W. Hage, A. Hallbrucker, G.P. Johari, E. Mayer, J. Chem. Phys. 104 (1996) 414.
[118] G.P. Johari, Phys. Chem. Chem. Phys. 7 (2005) 1091.
[119] G.P. Johari, J. Chem. Phys. 122 (2005) 144508.
[120] D.W. Davidson, R.H. Cole, J. Chem. Phys. 19 (1951) 1484.
[121] N. Hill, W.E. Vaughan, A.H. Price, M. Davies, Dielectric Properties and Molecular Behaviour, Von Nostrand, London, 1969.
[122] K.S. Cole, R.H. Cole, J. Chem. Phys. 9 (1941) 341.
[123] K. Okada, M. Yao, Y. Hiejima, H. Kohno, Y. Kajihara, J. Chem. Phys. 110 (1999) 3026.
[124] S. Kawada, J. Phys. Soc. Jpn. 57 (1988) 3694.
[125] O. Yamamuro, M. Oguni, T. Matsuo, H. Suga, J. Phys. Chem. Solids 48 (1987) 935.
[126] Y.P. Handa, D.D. Klug, E. Whalley, J. Phys. Colloq. 48 (1987) 435.
[127] Y.P. Handa, D.D. Klug, E. Whalley, Can. J. Chem. 66 (1988) 919.
[128] O. Yamamuro, M. Oguni, T. Matsuo, H. Suga, J. Phys. Chem. Solids 49 (1988) 425.
[129] G.P. Johari, J. Chem. Phys. 119 (2003) 2935.
[130] C.G. Salzmann, I. Kohl, T. Loerting, E. Mayer, A. Hallbrucker, Phys. Chem. Chem. Phys. 5 (2003) 3507.
[131] G.P. Johari, A. Hallbrucker, E. Mayer, Science 273 (1996) 90.
[132] C.G. Salzmann, P.G. Radaelli, A. Hallbrucker, E. Mayer, J.L. Finney, Science 311 (2006) 1758.
[133] M.M. Koza, B. Geil, H. Schober, F. Natali, Phys. Chem. Chem. Phys. 7 (2005) 1423.
[134] G.P. Johari, J. Chem. Phys. 117 (2002) 2782.
[135] M. Fisher, J.P. Devlin, J. Phys. Chem. 99 (1995) 11584.
[136] G.P. Johari, J. Phys. Chem. B 102 (1998) 4711.
[137] M. Chonde, M. Brindza, V. Sadtchenko, J. Chem. Phys. 125 (2006) 094501.
[138] C. Alba, L.E. Busse, C.A. Angell, J. Chem. Phys. 92 (1990) 617.
[139] W. Pascheto, M.G. Parthun, A. Hallbrucker, G.P. Johari, J. Non-Cryst. Solids 171 (1994) 182.
[140] G.P. Johari, Philos. Mag. 35 (1977) 1077.
[141] A. Hallbrucker, E. Mayer, G.P. Johari, Phil. Mag. B 60 (1989) 179.
[142] G.P. Johari, G. Fleissner, A. Hallbrucker, E. Mayer, J. Phys. Chem. 98 (1994) 4719.
[143] B.J. Skinner, J.J. Fahey, J. Geophys. Res. 68 (1963) 5595.
[144] R. Schrader, W. Dusdorf, Krist. Technol. 1 (1966) 59.
[145] W. Primak, The Compacted States of Vitreous Silica, Studies of Radiation Effects in Solids, Gordon and Breach, London, 1975.
[146] L.H. Brixner, Mater. Res. Bull. 7 (1972) 879.
[147] A.Y. Yarmakov, Y. Yurchikov, V.A. Barinov, Phys. Met. Metall. (English Transl.) 52 (1981) 50.
[148] C.C. Koch, O.B. Cavin, C.J. McKamey, J.O. Scarborough, Appl. Phys. Lett. 43 (1983) 1017.
[149] R.J. Hemley, A.P. Jephcoat, H.K. Mao, L.C. Ming, M.H. Manghnani, Nature 334 (1988) 52.
[150] G.P. Johari, O. Andersson, in: S.J Rzoska, V.M. Mazur (Eds.), Proceedings of NATO ARW on Soft Matter under Exogenic Impacts, NATO Science Series II: Mathematics, Physics and Chemistry, vol. 242, Springer, Berlin, 2007, pp. 33–72.
[151] L. Bosio, G.P. Johari, M. Oumezzine, J. Teixeira, Chem. Phys. Lett. 188 (1992) 13.
[152] G.P. Johari, O. Andersson, Phys. Rev. B 70 (2004) 184108.
[153] T. Loerting, W. Schustereder, K. Winkel, C.G. Salzmann, I. Kohl, E. Mayer, Phys. Rev. Lett. 96 (2006) 025702.
[154] T. Loerting, C.G. Salzmann, K. Winkel, E. Mayer, Phys. Chem. Chem. Phys. 8 (2006) 2810.
[155] Y.P. Handa, J.S. Tse, D.D. Klug, E. Whalley, J. Chem. Phys. 94 (1991) 623.
[156] L. Bosio, G.P. Johari, J. Teixeira, Phys. Rev. Lett. 56 (1986) 460.
[157] Y. Yoshimura, H. Kanno, Chem. Phys. Lett. 349 (2001) 51.
[158] O.V. Stal'gorova, E.L. Gromnitskaya, V.V. Brazhkin, JETP Lett. 62 (1995) 356.
[159] E.L. Gromnitskaya, O.V. Stal'gorova, V.V. Brazhkin, JETP Lett. 85 (1997) 109.

[160] O.V. Stal'gorova, E.L. Gromnitskaya, V.V. Brazhkin, A.G. Lyapin, JETP Lett. 69 (1999) 694.
[161] O. Mishima, H. Stanley, Nature 392 (1998) 164.
[162] C.K. Majumdar, Solid State Commun. 9 (1971) 1987.
[163] J.T. Bendler, M.F. Schlesinger, Macromolecules 18 (1985) 591.
[164] G.W. Scherrer, Relaxations in Glasses and Composites, John Wiley, New York, 1986.
[165] K. Schmidt, Rohr, H.W. Spiess, Phys. Rev. Lett. 66 (1991) 3020.
[166] B. Schiener, R. Bohmer, A. Loidl, R.V. Chamberlin, Science 274 (1996) 752.
[167] M. Cicerone, F.R. Blackburn, M.F. Ediger, J. Chem. Phys. 102 (1995) 471.
[168] A. Plonka, Dispersive Kinetics, Kluwer, Dordrecht, 2001.
[169] Y. Yoshimura, H.-K. Mao, R.J. Hemley, Chem. Phys. Lett. 420 (2006) 503.
[170] G.P. Johari, H.A.M. Chew, Philos. Mag. B 49 (1984) 647.
[171] R.J. Hemley, L.C. Chen, H.K. Mao, Nature 338 (1989) 638.
[172] M.A. Floriano, Y.P. Handa, D.D. Klug, E. Whalley, J. Chem. Phys. 91 (1989) 7187.
[173] G.P. Johari, Philos. Mag. B 80 (2000) 323.
[174] M. Scheuermann, B. Geil, K. Winkel, F. Fujara, J. Chem. Phys. 124 (2006) 224503.
[175] S.K. Sikka, J. Phys. Condens. Matter 16 (2004) S1033.
[176] T. Strassle, A.M. Saitta, S. Klotz, M. Braden, Phys. Rev. Lett. 93 (2004) 225901.
[177] J. Zhang, Y. Zhao, H. Xu, M.V. Zrelinskas, L. Wang, Y. Wang, T. Uchida, Chem. Mater. 17 (2005) 2817.
[178] C.A. Perottoni, J.A.H. da Jornada, Science 280 (1998) 886.
[179] G.P. Johari, E. Whalley, J. Chem. Phys. 75 (1981) 1333.
[180] G.P. Johari, W. Pascheto, S.J. Jones, J. Chem. Phys. 100 (1994) 4548, and references therein.
[181] G. Salvetti, E. Tombari, G.P. Johari, J. Chem. Phys. 102 (1995) 4987.
[182] M. Born, K. Huang, Dynamic Theory of Crystal Lattices, Clarendon, Oxford, 1954.
[183] J.S. Tse, D.D. Klug, C.A. Tulk, I. Swainson, E.C. Svensson, C.K. Loong, V. Shpakov, V.R. Belosludov, R.V. Belosludov, Y. Kawazoe, Nature 400 (1999) 647.
[184] J. Perez, C. Mai, R. Vassoile, J. Glaciol. 21 (1977) 361.
[185] C.A. Coulson, D. Eisenberg, Proc. Roy. Soc. (Lond.) A 291 (1966) 454.
[186] G.P. Johari, S.J. Jones, J. Chim. Phys. Phys.-Chim. Biol. (Fr.) 82 (1985) 1019.
[187] M. Nagahama, H. Suga, O. Andersson, Thermochim. Acta 363 (2000) 165.
[188] S. Furukawa, M. Nagahama, H. Suga, High Temp.-High-Press. 32 (2000) 397.
[189] T.G. Richards, G.P. Johari, Philos. Mag. B 58 (1988) 445.
[190] T. Loerting, I. Kohl, C. Salzmann, E. Mayer, A. Hallbrucker, J. Chem. Phys. 116 (2002) 3171.
[191] O. Yamamuro, I. Tsukushi, T. Matsuo, J. Mol. Cryst. Liquid Cryst. 277 (1996) 205.
[192] H. Suga, J. Phys.: Condens. Matter 15 (2003) S775.
[193] M.H. Bhat, I. Peral, J.R.D. Copley, C.A. Angell, J. Non-Cryst. Solids 352 (2006) 4517.
[194] R. Rao, T. Sakuntala, B.K. Godwal, Phys. Rev. B 65 (2002) 054108.
[195] R. Rao, T. Sakuntala, A.K. Arora, S.K. Deb, J. Chem. Phys. 121 (2004) 7320.
[196] M. Koza, H. Schober, A. Tölle, F. Fujara, T. Hansen, Nature 397 (1999) 661.
[197] T. Loerting, I. Kohl, W. Schustereder, K. Winkel, E. Mayer, Chem. Phys. Chem. 7 (2006) 1203.
[198] R.J. Nelmes, J.S. Loveday, T. Strässle, C.L. Bull, M. Guthrie, G. Hamel, S. Klotz, Nat.-Phys. 2 (2006) 414.
[199] Y. Suzuki, Phys. Rev. B 70 (2004) 172108.